

MINCLE and TLR9 agonists synergize to induce Th1/Th17 vaccine memory and mucosal recall in mice and non-human primates

Received: 14 March 2024

Accepted: 24 September 2024

Published online: 17 October 2024

 Check for updates

Joshua S. Woodworth¹✉, Vanessa Contreras², Dennis Christensen¹, Thibaut Naninck², Nidhal Kahlaoui², Anne-Sophie Gallouët², Sébastien Langlois², Emma Burban², Candie Joly², Wesley Gros², Nathalie Dereuddre-Bosquet², Julie Morin², Ming Liu Olsen¹, Ida Rosenkrands¹, Ann-Kathrin Stein³, Grith Krøyer Wood³, Frank Follmann¹, Thomas Lindenstrøm¹, Tu Hu¹, Roger Le Grand², Gabriel Kristian Pedersen¹ & Rasmus Mortensen¹✉

Development of new vaccines tailored for difficult-to-target diseases is hampered by a lack of diverse adjuvants for human use, and none of the currently available adjuvants induce Th17 cells. Here, we develop a liposomal adjuvant, CAF[®]10b, that incorporates Mincle and Toll-like receptor 9 agonists. In parallel mouse and non-human primate studies comparing to CAF[®] adjuvants already in clinical trials, we report species-specific effects of adjuvant composition on the quality and magnitude of the responses. When combined with antigen, CAF[®]10b induces Th1 and Th17 responses and protection against a pulmonary infection with *Mycobacterium tuberculosis* in mice. In non-human primates, CAF[®]10b induces higher Th1 responses and robust Th17 responses detectable after six months, and systemic and pulmonary Th1 and Th17 recall responses, in a sterile model of local recall. Overall, CAF[®]10b drives robust memory antibody, Th1 and Th17 vaccine-responses via a non-mucosal immunization route across both rodent and primate species.

Adjuvants are immunostimulators that are included in vaccines to enhance the magnitude, phenotype, and longevity of the resulting immune responses. With scientific advancements, the list of licensed vaccines using adjuvants has grown and includes subunit vaccines against human papillomavirus, hepatitis B, pandemic influenza, malaria, shingles disease and SARS-CoV-2. However, since the introduction of alum in the 1920s, only a handful of new adjuvants have become available for human use¹. This significantly hampers the development of novel vaccines and there is a recognized need for

diversification in the portfolio of available adjuvants/vaccine platforms^{2,3}.

In the ideal scenario, different adjuvants could be used to tailor the immune responses for specific needs, but the mechanisms by which many of the existing adjuvants work and the functional responses they induce are only partially understood¹. For instance, few of the available adjuvants were initially designed to induce robust T cell responses, and it has proven challenging to specifically direct cellular immune functionalities. Of particular interest, despite the

¹Department of Infectious Disease Immunology, Statens Serum Institut, Artillerivej 5, 2300 Copenhagen, Denmark. ²Université Paris-Saclay, Inserm, CEA, Immunologie des maladies virales, auto-immunes, hématologiques et bactériennes (IMVA-HB/IDMIT/UMR1184), 92265 Fontenay-aux-Roses & Kremlin Bicêtre, France. ³Department of Vaccine Development, Statens Serum Institut, Artillerivej 5, 2300 Copenhagen, Denmark. ✉e-mail: jow@ssi.dk; rjm@ssi.dk

growing evidence of a protective role of Th17 cells against both viral and bacterial infections, such as influenza, *Bordetella pertussis* and *Mycobacterium tuberculosis* (Mtb)^{4–12}, the available human adjuvants have not been shown to induce a detectable Th17 responses. Although there are pre-clinical examples of adjuvants that induce vaccine-specific Th17 responses when given via a mucosal administration route^{13–15}, Th17 induction by adjuvanted subunit vaccine via traditional intramuscular (IM) and subcutaneous (SC) parenteral routes is limited and not defined outside small animal models¹⁶. Therefore, together with increasing the overall magnitude of cellular immune responses, specific induction of Th17 cells is a prime goal for vaccine optimization strategies. With a greater understanding of immune signaling pathways and advancements in synthetic chemistry, there is a possibility to design highly specialized adjuvants that can be manufactured from widely available constituents.

The cationic adjuvant formulation (CAF[®]) family consists of well-defined stable liposomes that facilitate co-delivery of antigen and immunostimulator to target cells and slow antigen release by forming depots at the injection site¹⁷. They consist of all-synthetic components, making the CAF[®] platform an optimal starting point for developing the next generation of safe and immunogenic adjuvants. Furthermore, several CAF[®] adjuvants are able to stimulate Th17 responses after subcutaneous immunization in mice^{17,18}. The first member of the family, CAF[®]01, consisting of dimethyldioctadecylammonium (DDA) and the Mincle agonist Trehalose-6,6-dibehenate (TDB), has completed 5 clinical trials and has been shown to induce 5–6 fold higher IgG titers than aluminum hydroxide and stable cell-mediated immune (CMI) responses for more than 150 weeks in humans^{19,20}. However, for some disease targets, a stronger CMI response is desirable, and encouraged by the clinical success of the highly immunogenic AS01[®] adjuvant in shingles, malaria, and tuberculosis (TB) vaccines^{21,22}. The goal of this study was therefore to develop and test a next-generation CAF[®] adjuvant displaying increased long-term CMI responses, while supporting vaccine-priming of Th17 cells. Such an adjuvant would have a broad range of applications, including vaccines for respiratory infections, where Th17 cells are described to form resident memory T cells and accelerate local immune responses^{23,24}. It would therefore also be the ideal candidate to be co-developed with the recently introduced tuberculosis vaccine antigen, H107, from our group²⁵.

Here we introduce a potent CAF[®] adjuvant formulation, CAF[®]10b, that incorporates TLR9 and Mincle agonists and is shown to induce robust Th17 responses in both mice and non-human primates (NHPs). CAF10b is systematically compared head-to-head in mice and NHPs against three other CAF[®] adjuvants; *i*) CAF[®]01, included as a benchmark adjuvant with clinical data and comparative results to other adjuvants approved for human use^{19,20,26,27}, *ii*) CAF[®]09b, which incorporates the TLR3 agonist poly(I:C) and is in clinical trials for prevention of chlamydia (NCT03926728) and cancer immunotherapy²⁸, and *iii*) an experimental higher-dose formulation of CAF[®]09b (CAF[®]09^{hi}). We observe that CAF[®]01 and CAF[®]10b give the highest cellular immune responses in mice, including significant Th1 and Th17 responses, with functional protective capacity against murine Mtb infection, as an example of a difficult-to-target disease. Compared to CAF[®]01, CAF[®]10b increases the memory responses in the NHPs, defined by its ability to induce Th1 together with Th17 cells. The CAF[®]09^{hi} formulation gave the highest peak Th1 response, but ultimately a lower detectable memory response than CAF[®]10b, demonstrating that peak cellular immune responses do not necessarily reflect memory responses. When animals were exposed to antigen six months after vaccination to study functional memory recall, CAF[®]-induced T cells showed potent systemic expansion and ability to migrate into local tissues, including the lung mucosa. These data are highly encouraging towards filling an important immunological gap in modern vaccine development. Our study also demonstrates local antigen recall as a

feasible translational approach to evaluating vaccines in the absence of a human challenge model.

Results

Incorporation of human TLR9 agonist CpG2006 into DDA/MMG makes stable liposomes that induce Th1/Th17 responses in mice
As a starting point for our efforts to develop a new CAF[®] formulation with increased CMI responses, we investigated the effect of incorporation of TLR agonists into Mincle-activating liposomes composed of dimethyldioctadecylammonium/monomycoloyl glycerol (DDA/MMG)¹⁷ on CMI responses to an adsorbed protein antigen. We observed that co-agonism of TLR9, but not TLR4 or TLR7, increased the relative vaccine-induced Th1 (IFN γ) and Th17 (IL-17A) responses in mice (Fig. 1A). This confirmed previous studies demonstrating a beneficial effect of incorporating CpG1826 into DDA/MMG liposomes in mice²⁹. However, as CpG1826 is a weak ligand for human TLR9, we explored the use of CpG2006, which has been validated in human clinical trials^{30,31}. Using HEK-293 cells expressing the human TLR9 gene and an NF- κ B-driven SEAP reporter, we confirmed that CpG2006 stimulated human TLR9 while CpG1826 did not (Fig. 1B). Moreover, we found that CpG2006 also stimulated HEK-293 cells expressing murine TLR9, demonstrating potential adjuvant properties across species.

We next incorporated CpG2006 into CAF[®] liposomes and studied responses in mice. Incorporation of CpG2006 into the DDA/MMG liposomes synergistically increases adjuvant-induced IFN γ and IL-17A responses compared to CpG2006 or DDA/MMG alone (Fig. 1C), while also significantly reducing systemic inflammation associated with administering free CpG2006 (Fig. S1A). To establish a more optimal vaccine dose of CpG in DDA/MMG liposomes, CB6F1 mice were subcutaneously (SC) immunized with antigen adsorbed to liposomes with increasing CpG concentrations and analyzed two weeks after the last immunization for IFN γ and IL-17 release from antigen-stimulated splenocytes. Consistent with our initial results (Fig. 1A, C), incorporation of CpG2006 into DDA/MMG increased both Th1 and Th17 responses (Fig. 1D, left), whereas CpG alone did not induce Th17 responses (Fig. 1C and S1B). There was a clear dose dependency, with the highest dose of CpG2006 (50 μ g) giving the highest responses (Fig. 1D, left). In contrast, CpG1826 demonstrated the highest responses at the intermediate dose of 2 μ g, with lower responses at the 50 μ g dose. This suggests that adjuvant-overdosing of CpG with respect to CMI is possible, in particular in settings where the TLR9 recognition of the CpG motif is strong, such as CpG1826 in mice (Fig. 1B), which is consistent with the tolerogenic effects of high dose CpG in vitro³². We therefore aimed for an intermediate immunogenic dose of CpG2006 for the final formulation to be used in NHPs/humans and observed that a 25:5:2 DDA/MMG/CpG2006 ratio resulted in highly stable liposomes (denoted CAF[®]10b). CAF[®]10b liposomes had an average size of 250–300 nm and a net positive charge (Fig. 1E, right), similar to existing CAF[®] adjuvants. Importantly, long-term stability studies at 2–8 °C demonstrated a minimal increase in liposome size and no decline in CpG, DDA, or MMG concentrations over a twelve-month period (Fig. S2A–E).

In summary, formulation of CpG2006 with DDA/MMG increases CAF[®]-induced Th1 and Th17 responses in mice.

CAF[®]01 and CAF[®]10b induce similar vaccine responses and protection against *M.tuberculosis* challenge in mice

Having developed stable CAF[®]10b liposomes, we next tested the functional capacity of the immune response to protect against a respiratory infection. For this, we utilized the recently developed TB vaccine antigen H107²⁵ to make head-to-head comparisons against existing CAF[®] adjuvants in the mouse model (Fig. 2A). CAF[®]01 has previously been shown to induce antibody, Th1, and Th17 responses in mice²⁶ and was chosen for direct comparison to CAF[®]10b. In addition,

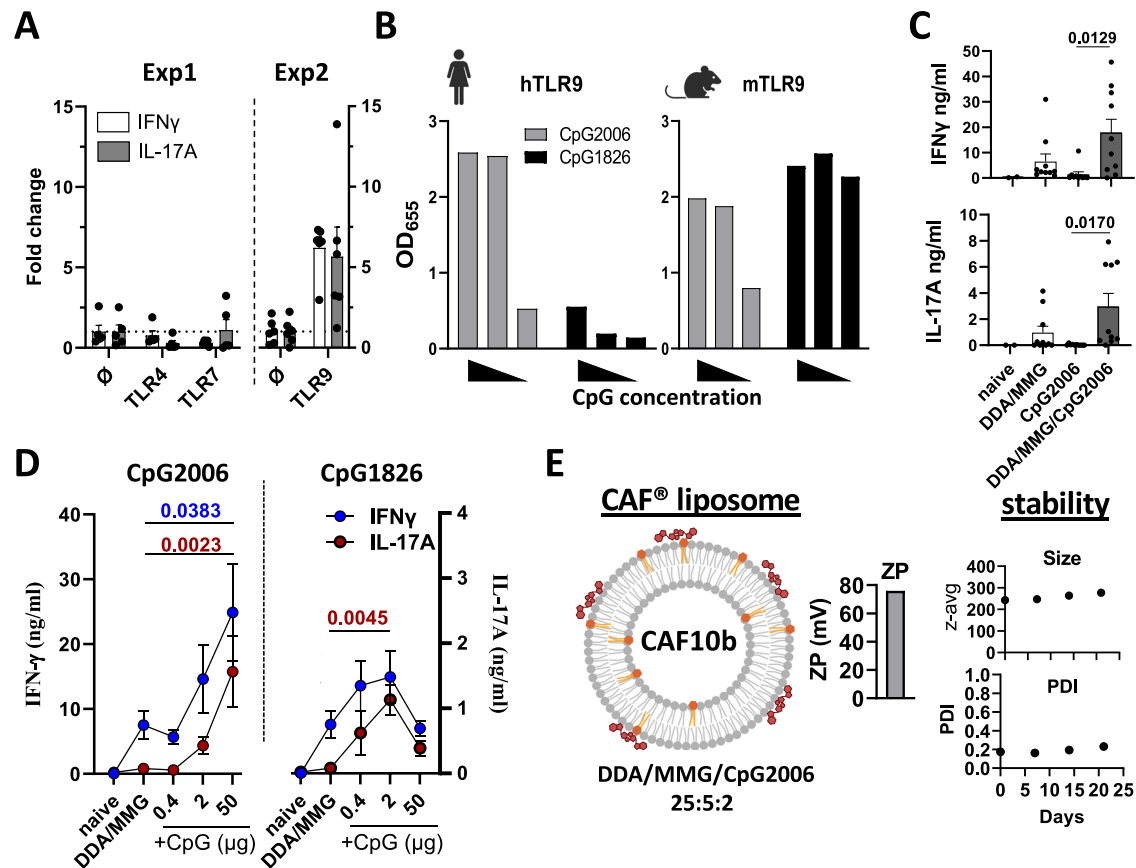


Fig. 1 | TLR9 agonists increase CAF[®]-mediated Th1/Th17 responses in mice. **A** CB6F1 mice immunized 2x SC with H56 protein antigen adsorbed to DDA/MMG liposomes alone (∅) or combined with various TLR agonists (TLR4, monophosphoryl lipid; TLR7, 3M-052; TLR9, CpG1826) in independent experiments and assessed after 2 weeks by antigen stimulation of splenocytes for IFN γ and IL-17 A secretion by ELISA. Bars, mean \pm SD fold change compared to DDA/MMG alone (∅). Symbols, individual mice, $n = 5$ /grp (Exp1) $n = 67$ grp (Exp2). **B** HEK-Blue[™] reporter cells expressing human TLR9 (left) or murine TLR9 (right) were stimulated in vitro with decreasing concentrations (100, 10, 1 μ g/ml) of CpG2006 (grey bars) or CpG1826 (black bars) for 17 hrs and supernatants assayed for SEAP activity by HEK-Blue detection QUANTI-Blue[™] (shown as OD₆₅₅). The experiment was performed twice. **C** Splenocytes from CB6F1 mice immunized 2x SC with H56 protein

combined with 10 μ g CpG2006 alone or DDA/MMG liposomes \pm 10 μ g CpG2006 assessed 2 weeks after immunization for IFN γ and IL-17A secretion by ELISA. Bars, mean \pm SD; symbols, individual mice $n = 10$ /grp and $n = 2$ naive, ANOVA with Tukey's posttest adjusted for multiple comparisons, p values < 0.1 shown. **D** CB6F1 mice immunized 2x SC with DDA/MMG liposomes combined with various amounts of CpG2006 (left) or CpG1826 (right) adsorbed with H56 protein antigen, and two weeks later, PBMCs stimulated ex vivo with protein antigen to assess secreted IFN γ (blue) and IL-17A (red) by ELISA. Symbols indicate mean \pm SD, $n = 8$ /grp and $n = 2$ naive, ANOVA with Dunnett's posttest adjusted for multiple comparisons, p values < 0.1 shown. **E** The depicted CAF[®]10b adjuvant was assessed for zeta potential (ZP) (left), particle size (top right) and polydispersity index (bottom right) over 25 days. Source data are provided as a Source Data file.

two formulations of CAF[®]09³³, DDA/MMG liposomes containing the TLR3 agonist Poly(I:C), with two-fold dose variation of MMG/poly(I:C) (CAF[®]09^{lo} and CAF[®]09^{hi}) were also included to allow for investigation of the relative effects of TLR3 agonist incorporation. The adjuvants CAF[®]01 and CAF[®]09^{lo} (also called CAF[®]09b) are currently in clinical development^{17,20,28}. All H107/CAF[®] formulations induced H107-specific antibody responses in mice (Fig. S3). Serum anti-H107 IgG levels were similar amongst all adjuvants, while isotyping revealed lower IgG1 levels in CAF10b-immunized mice and lower IgG2c levels in CAF01- and CAF09^{hi}-immunized mice. All H107/CAF[®] vaccines induced vaccine-specific CD4 T cells, including IFN γ -producing (Th1) and IL-17A-producing (Th17) responses (Fig. 2B). CAF[®]01 and CAF[®]10b were the most effective at inducing vaccine-specific Th1/Th17 responses, while the CAF[®]09 formulations were less immunogenic, inducing significantly lower Th1 and Th17 responses (Fig. 2B, C, D). The Th1 and Th17 responses observed by the parallel ICS and cytokine secretion ELISAs showed similar relative hierarchy between the adjuvants, with the IL-17A ELISA demonstrating enhanced sensitivity of Th17 responses (Fig. 2B, C, D). To compare the functional capacity of the immune responses, we applied the murine aerosol Mtb infection model, where a combined Th1/Th17 response is suggested to be optimal for

protection^{15,25,26,34,35}, and in which H107/CAF[®]01 provides reduction in bacterial burden lung and spleen similar to BCG²⁵ (Fig. S4A). Indeed, following aerosol challenge with Mtb, H107 adjuvanted with either CAF[®]01 or CAF[®]10b provided the greatest CFU reduction (2.53 log and 2.32 log, respectively, compared to control animals) (Fig. 2E), with a similar relative pattern of CFU in the spleen (Fig. S4B).

In summary, H107/CAF[®]10b induced similar antigen-specific Th1/Th17 responses comparable to H107/CAF[®]01 and provided robust protection against Mtb aerosol challenge in mice.

CAF[®] adjuvants induce robust antibody responses in non-human primates

To assess their relative translational potential, we sought to directly compare the induction of cellular and humoral immunogenicity these CAF[®] adjuvants in NHPs. Paralleling the mouse studies, the H107 antigen was combined with either CAF[®]10b, CAF[®]01, CAF[®]09^{lo}, or CAF[®]09^{hi} (Fig. 3). CAF[®]01 served as a benchmark in these studies as it has previously been combined with several antigens, including the tuberculosis vaccine antigen H56 and the chlamydia antigen CTH522 in NHP immunization studies and in clinical trials^{19,20,27,36,37}. The vaccines were given as a two-dose intramuscular immunization regimen with

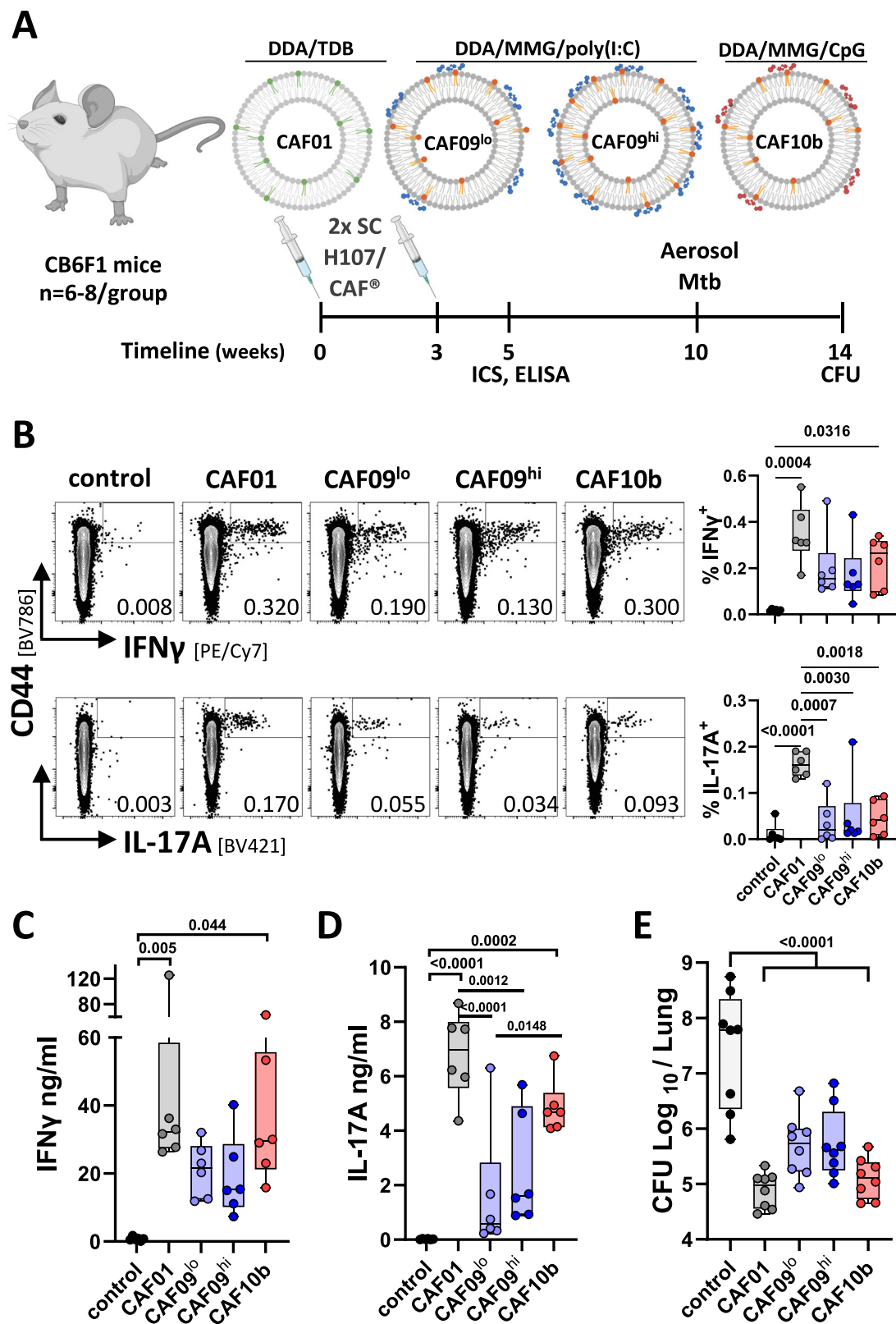


Fig. 2 | CAF[®] induction of Th1 and Th17 responses in mice. **A** CB6F1 mice were immunized with the H107 antigen adsorbed to different CAF[®] adjuvants as depicted. **B–D** Splenocytes taken 2 weeks after the last immunization of control ($n=4$) and H107/CAF[®]-immunized mice ($n=6$ /group) were stimulated ex vivo with H107. **B** Analysis of CD4 T cells following ICS assay from each vaccine group showing representative dot plots (left) where the number shown depicts % cytokine positive

CD4 T cells (singlets \rightarrow live \rightarrow lymphocytes \rightarrow CD3⁺ \rightarrow CD8⁻, CD4⁺) and bar plots (right). **C, D** ELISAs for IFN γ **C** and IL-17A **D** secretion from H107-stimulated splenocytes. **E** Bacterial load in the lungs of control and H107/CAF[®]-immunized mice ($n=8$ /group) 4 weeks after aerosol Mtb infection. **B–E** Symbols display individual mice; Bars represent median, IQR, min. and max values. P values, one-way ANOVA with Tukey's posttest. Source data are provided as a Source Data file.

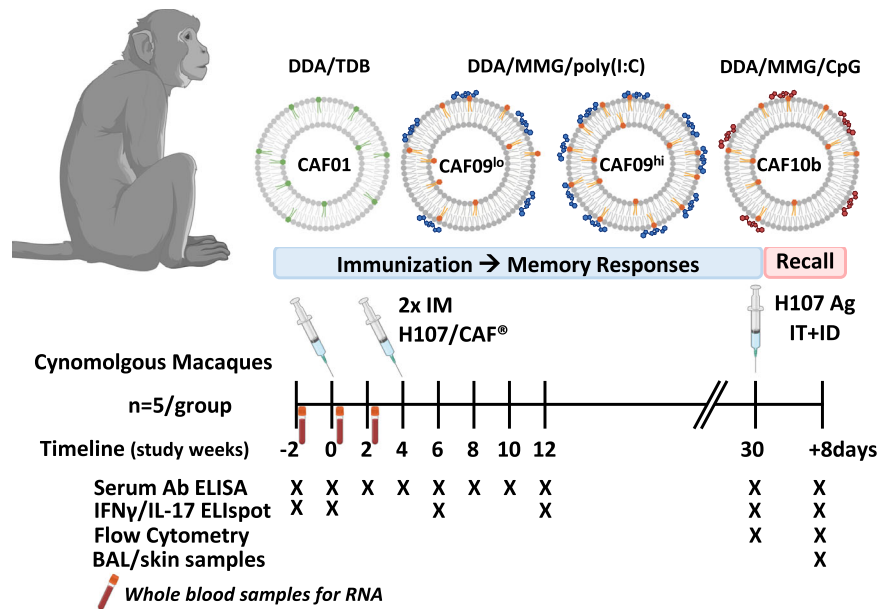


Fig. 3 | CAF[®] adjuvant comparison in Non-Human Primates. Cynomolgus macaques were immunized with the H107 antigen adsorbed to different CAF[®] adjuvants as depicted. Animals were monitored for baseline, initial, and memory

immune responses in the blood (serum, PBMC). In the antigen recall phase, animals were administered non-adsorbed H107 protein antigen into the lung and skin and the systemic (serum, PBMC) and local (skin, BAL) recall responses assessed.

four weeks spacing in cynomolgus macaques (Fig. 3). CMI and humoral immune responses were determined from blood samples taken at baseline prior to immunization and at multiple time points, including 6 months, after the final immunization (Fig. 3). Overall, all four CAF[®] adjuvants were well-tolerated. A transient increased body temperature on the day after each immunizations, typically 0–2 °C, was observed for immunized NHPs, with the highest temperature changes in the CAF[®]10b group. Otherwise, vaccinated animals did not vary noticeably relative to saline controls (Fig. S5A). Similarly, overall weight changes were not different amongst the immunized groups (Fig. S5B), and complete blood counts taken bi-weekly over the study's course did not show measurable differences in white blood cellular composition (Fig. S5C, D).

All adjuvants induced H107-specific IgG in the serum of NHPs after the first immunization, which was further boosted after the second immunization (Fig. 4A). Peak anti-H107 IgG responses were achieved 2 weeks after the booster for all groups (wk6 post 1st immunization), wherein H107/CAF[®]10b and H107/CAF09^{hi} induced greater than 2-fold higher IgG relative to H107/CAF[®]01, with increases of 0.323 log and 0.374 log, respectively (Fig. 4B). The median serum anti-H107 IgG levels induced by CAF[®]10b and CAF09^{hi} remained consistently higher than CAF[®]01 and CAF[®]09^{lo} at all time points investigated (Fig. 4A). Cumulative IgG responses over the 30-week follow-up period of the study confirmed induction of significant responses versus non-immunized control animals (Fig. 4C). Serum H107-specific IgA was detected after the second immunization in animals immunized with CAF[®]01, CAF[®]09^{hi}, and CAF[®]10b (Fig. 4E, F). However, the kinetics of sustained antibody responses varied, and when integrated over 30 weeks, only H107 adjuvanted with CAF[®]09^{hi} and CAF[®]10b demonstrated a significant IgA response (Fig. 4F).

Overall, all CAF[®] adjuvants investigated induced vaccine-specific antibody responses, with CAF[®]09^{hi} and CAF[®]10b displaying both the highest peak and sustained antigen-specific IgG and IgA responses.

CAF[®]10b induces long-term Th1 and Th17 responses in NHPs

The primary focus of this study was to investigate the CMI-inducing capacity of these adjuvants, including Th1 and Th17 responses. Therefore, we prioritized sensitive IFN γ and IL-17A ELISpot assays over flow cytometry for the post-vaccination responses to maximize

potential detection of Th17 responses that are rarely present in blood^{38,39}. H107 antigen stimulation of PBMCs using overlapping peptides revealed systemic antigen-specific IFN γ responses in all vaccine adjuvant groups, with the peak response detected two weeks after the final immunization (six weeks post first immunization), after which there was a contraction of responses (Fig. 5A). At peak, CAF[®]09^{hi} and CAF[®]10b showed the highest vaccine-specific IFN γ responses, with 5 out of 5 animals displaying spot-forming cell (SFC) counts above those of any control animal compared to 3 of 5 for CAF[®]01 and CAF[®]09^{lo} (Fig. 5A). Interestingly, at 30 weeks post first immunization, only the H107/CAF[®]10b-immunized group had a significant detectable IFN γ ELISpot response, indicating sustained long-term CMI responses in circulation. H107-specific IL-17A ELISpot results after H107 protein stimulation demonstrated vaccine-specific responses with similar kinetics to IFN γ , wherein individual animals in all immunization groups demonstrated vaccine-specific IL-17A responses two weeks after the final immunization (Fig. 5B, left). At 30 weeks post immunization H107/CAF[®]10b displaying the most durable Th17 response, with 4 of 5 animals still having IL-17A SFC counts above those of any control animal compared to two of five for CAF[®]01 and CAF09^{lo} and none for CAF[®]09^{hi} (Fig. 5B, right).

Focusing on their dynamic differences in adaptive immune responses, we compared CAF[®]09^{hi} and CAF[®]10b for their initial immune “fingerprint” by transcriptomics of blood samples taken 1 day after each immunization. Principle Component Analysis (PCA) showed that CAF[®]09^{hi} animals separated further away from baseline (BL) compared to CAF[®]10b after the first immunization, whereas a high degree of overlap was seen after the booster vaccination (Fig. 5C). Indeed, 792 genes were already significantly upregulated over baseline after the first CAF[®]09^{hi} immunization in comparison to 322 genes by CAF[®]10b (Fig. S6A, B). As expected, the top variably expressed genes were associated with inflammatory cells and pathways (Fig. S6C), and gene set enrichment analysis (GSEA) relative to baseline using the reference set Gene Ontology Biological Process, identified several innate immunological gene sets as the highest scoring pathways (Fig. 5D, see Fig. S6D for annotated list). Subsequent targeted GSEA of related gene sets demonstrated increased activation of pathways associated pro-inflammatory macrophage activation, TNF and IFN γ , IL-1 and IL-6, regulatory IL-10 pathways, and several type I IFN pathways

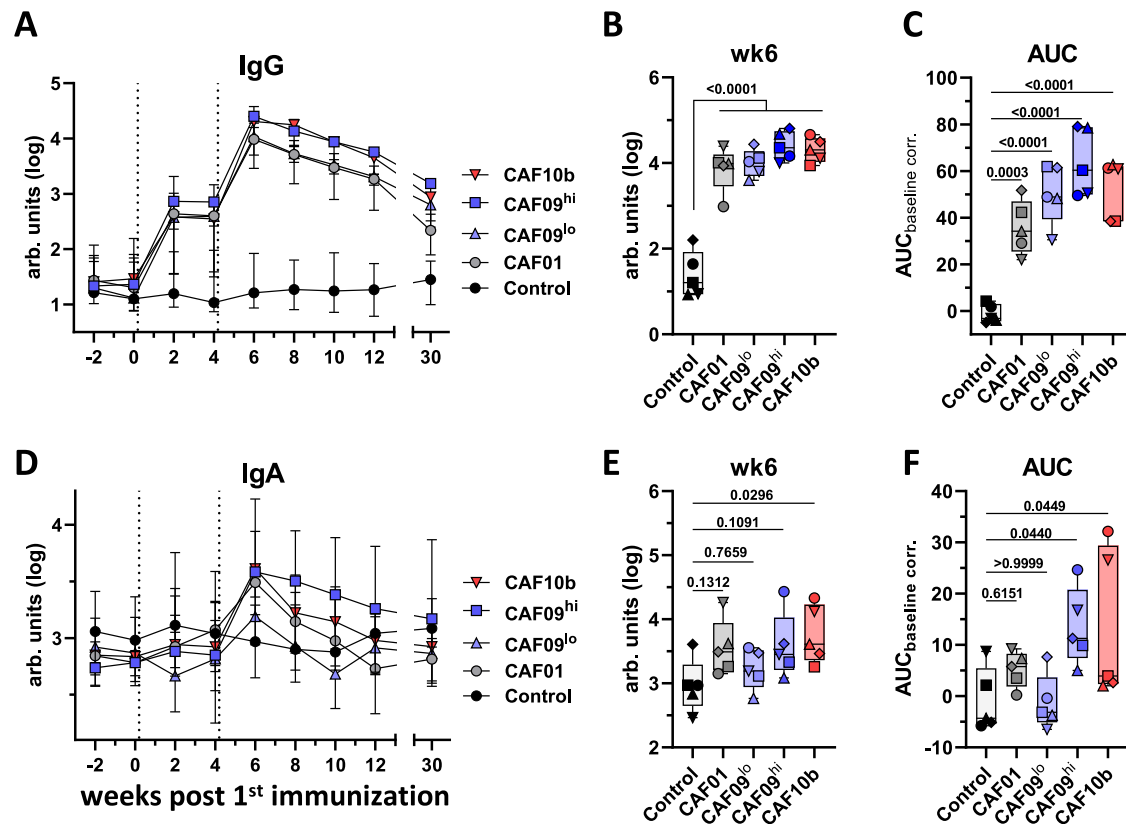


Fig. 4 | IgG and IgA responses are influenced by vaccine composition. H107-specific IgG **A–C** and IgA **(D–F)** antibody levels in the serum measured by ELISA before and after H107/CAF[®] immunization of non-human primates, $n = 5$ /group. **A, D** Immunizations are indicated by dotted lines. Symbols represent median \pm IQR of arbitrary units. **B, E** Peak responses at week 6. **C, F** Responses integrated over the

30-week time course calculated as area under the curve (AUC) after baseline subtraction are depicted. **B, C, E, F** Bars represent median \pm IQR, min. and max. Symbols, individual animals. P values, one-way ANOVA with Dunnett's post-hoc test adjusted for multiple comparisons of log-transformed data. Source data are provided as a Source Data file.

after the first CAF[®]09^{hi} immunization (Fig. 5D). Given the inhibitory effects of type I IFNs on Th17 induction^{40–43} and the TIR-domain-containing adapter-inducing interferon- β (TRIF) signaling by TLR3⁴⁴, we further investigated type I IFN induction by the CAF[®] adjuvants. Direct adjuvant stimulation of human THP-1 monocytic cells revealed that the TLR3-agonist containing CAF[®]09 formulations, but not CAF[®]01, CAF[®]10b or DDA/MMG control liposomes, activated type I IFN response factors (IRF) (Fig. 5E). Consistent with previously described TLR3-mediated induction of type I IFNs⁴⁴, IRF expression followed a poly(I:C) dose-dependent manner, CAF[®]09^{hi} > CAF[®]09^{lo}, (Fig. 7B), which may explain the observed decrease in Th17 induction by CAF[®]09^{hi} in NHPs.

In summary, immunization with the four CAF[®] adjuvants led to induction of CMI responses, with the highest Th1/Th17 memory responses observed for CAF[®]10b, six months after vaccination. Despite having the highest Th1 response at peak, CAF[®]09^{hi} displayed diminished Th17 responses, which may be linked to TLR3-dependent induction of Type I IFNs.

In vivo antigen delivery recalls local and systemic memory responses

Effective vaccine-memory is ultimately characterized by the capacity to mount a rapid recall response within relevant tissues. Therefore, after showing that the CAF adjuvants induced differential long-term memory in peripheral blood responses, we assessed their capacities to mount local and systemic recall responses. To prioritize a disease-agnostic approach with broad translational potential, we utilized an in vivo antigenic challenge model to assess recallable immune memory (Fig. 6A). Six months after the final immunization, H107 protein and an

irrelevant control protein (CTH522⁴⁵) were given intradermally at distal sites on each animal's upper back. Concurrently, H107 was given into the airways via bronchoscope instillation into the caudal right lung. Skin sites were monitored for delayed-type hypersensitivity (DTH) responses, where only a few immunized animals displayed minimal local redness and light swelling at the H107 injection sites (Fig. S7A). Additionally, to assess the local pulmonary inflammatory response of this model, a subset of NHP were subjected to sequential ¹⁸F-Fluorodesoxyglucose (¹⁸F-FDG) positron emission tomography with computed tomography (PET-CT) scanning before and after antigen instillation. Three Control animals were randomly selected to control for non-specific antigen instillation effects, and the group of CAF[®]10b-immunized animals were selected due to their high magnitude of H107-specific memory responses (Figs. 4, 5).

PET-CT analyses of the selected animals demonstrated highly localized pulmonary recall responses in the antigen-instilled right lungs of H107/CAF[®]10b-immunized NHP, but not in contralateral lungs or in control animals (Fig. 6B). Such responses were detectable as early as three days after instillation and were resolved by day seven post recall, demonstrating a short-lived local inflammatory response in this sterile recall model (Fig. 6C, Fig. S7B). Despite the intradermal antigen injection sites also being within the PET-CT scanning area, no local skin inflammatory responses were detected in these animals, consistent with a lack of observed DTH (Fig. S7A).

Eight days after antigen administration, all vaccine groups were assessed for local (skin/lung) and systemic recall responses. Antigen recall increased serum H107-specific IgG significantly in all vaccine groups, demonstrating a systemic booster response (Fig. 7A). Serum H107-specific IgA was also increased in the groups having received

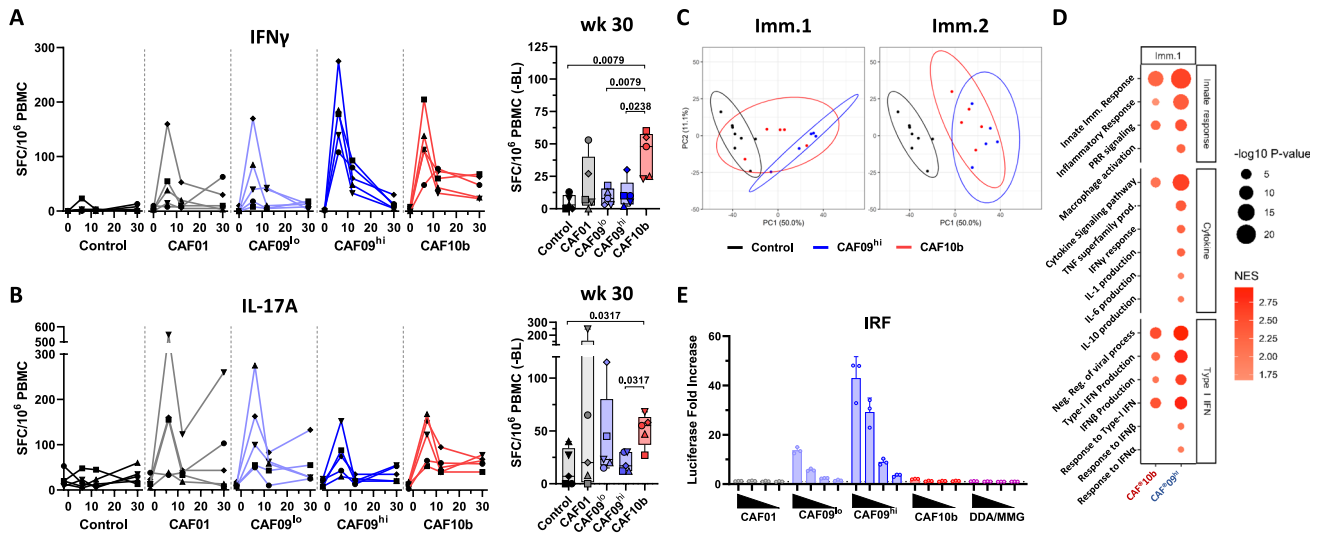


Fig. 5 | CAF® adjuvant induction of Th1 and Th17 responses and whole blood signatures differ in NHP. **A, B** PBMCs from immunized Non-human primates assessed by ELISpot before and after immunizations. PBMCs were stimulated ex vivo with an overlapping H107 peptide pool for **(A)** IFN γ or **(B)** H107-protein for IL-17A production. Symbols and lines indicate individual animals (left panels), $n = 5$ /group. Memory responses at 30 weeks post first immunization corrected for pre-immunization baseline SFC and plotted for each H107/CAF® immunized group (**A, B** right panels). Bars represent median \pm IQR, min. and max. Symbols, individual animals, $n = 5$ /group. P values shown from two-sided Mann-Whitney U tests. Kruskal-Wallis test **(A)** $p = 0.038$ **(B)** $p = 0.1253$. **C, D** Whole genome expression of immunized NHP assessed via mRNA sequencing of blood samples taken at baseline and one day after each immunization. **C** Principle components analysis (PCA)

comparing overall gene expression of baseline (black), H107:CAF10b (red), and H107:CAF09^{hi} (blue) after the first (Imm.1, left) or second (Imm.2, right) immunization. Symbols, individual NHP; circles, 95% confidence intervals. **D** Gene Set Enrichment Analyses (GSEA) of selected pathways. Normalized enrichment score (NES) calculated based on differential expression between imm.1 and baseline for individual animals normalized to mitigate differences of the gene set size; Kolmogorov–Smirnov-like two-tailed test with p-values adjusted by Benjamini–Hochberg method. **E** THP1-DualTM cells stimulated overnight with serial 2-fold dilutions of CAF® liposome formulations, from 25 μ g to 3.125 μ g/mL DDA, were assessed for induction of IRF-driven secreted luciferase. Bars, fold increase versus untreated cells, mean \pm SD of triplicates, representative data from two similar experiments. Source data are provided as a Source Data file.

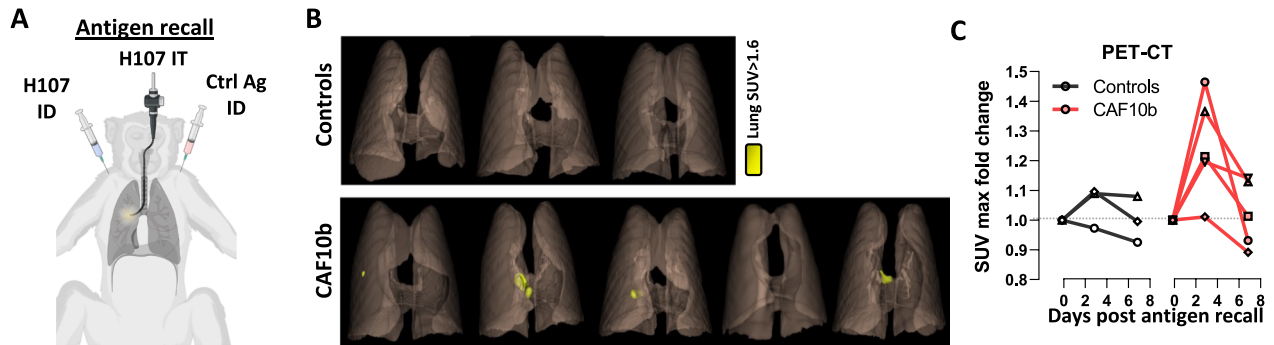


Fig. 6 | In vivo antigen delivery to vaccinated animals and transient local responses. Six months after the final immunization, non-human primates were given an in vivo antigen recall in the skin and lungs with H107, or a control protein, as shown in **A**. **B** PET-CT scans of H107/CAF®10b-immunized ($n = 5$) and randomly selected Control ($n = 3$) animals depicting local lung inflammatory responses 3 days

after H107 antigen recall, as standardized uptake value (SUV) > 1.6 . **C** The SUV maximum fold change relative to pre-recall (day 0) for the antigen-receiving lung lobes at 3 and 7 days after antigen recall for all the NHPs assessed by PET-CT. Source data are provided as a Source Data file.

CAF®01, CAF®10b and CAF®09^{hi}, but not CAF®09^{lo} (Fig. 7A), consistent with the pattern of antigen-specific IgA after immunization (Fig. 4D, F). In contrast, vaccine-specific IgG, but not IgA, was detected in bronchoalveolar lavage (BAL) fluid of all H107/CAF®-immunized groups compared to controls (Fig. S7C). Vaccine-specific antibodies were also assayed locally within the skin biopsies, however equal H107-specific IgG levels were detected in the biopsies taken at both the H107 and control protein sites, and therefore likely only reflected the systemic serum levels.

Systemic vaccine-specific CMI responses were also highly expanded by in vivo antigen recall. Notably, ELISpot analysis of PBMCs demonstrated a significant 19.6-fold median expansion (interquartile

range 11–50, $p = 0.0116$) in H107-specific IFN γ -producing (Th1) cells in H107/CAF®10b-immunized NHPs (Fig. 7B). IL-17A-secreting (Th17) cells were also greatly expanded in H107/CAF®10b animals ($p = 0.0435$) confirming the presence of recallable memory Th17 cells following immunization (Fig. 7C). Systemic Th1 and Th17 responses were also expanded in H107/CAF®01 and H107/CAF®09^{lo} animals. However, consistent with the lack of Th17 cells after initial H107/CAF®09^{hi} immunization (Fig. 5B), only Th1 responses were expanded in H107/CAF®09^{hi} animals (Fig. 7C).

Comparing the skin-infiltrating cells at the sites of H107 and control protein injection by flow cytometric analysis showed vaccine-specific CD4 T cell recall responses (Fig. 7D). Ex vivo H107 stimulation

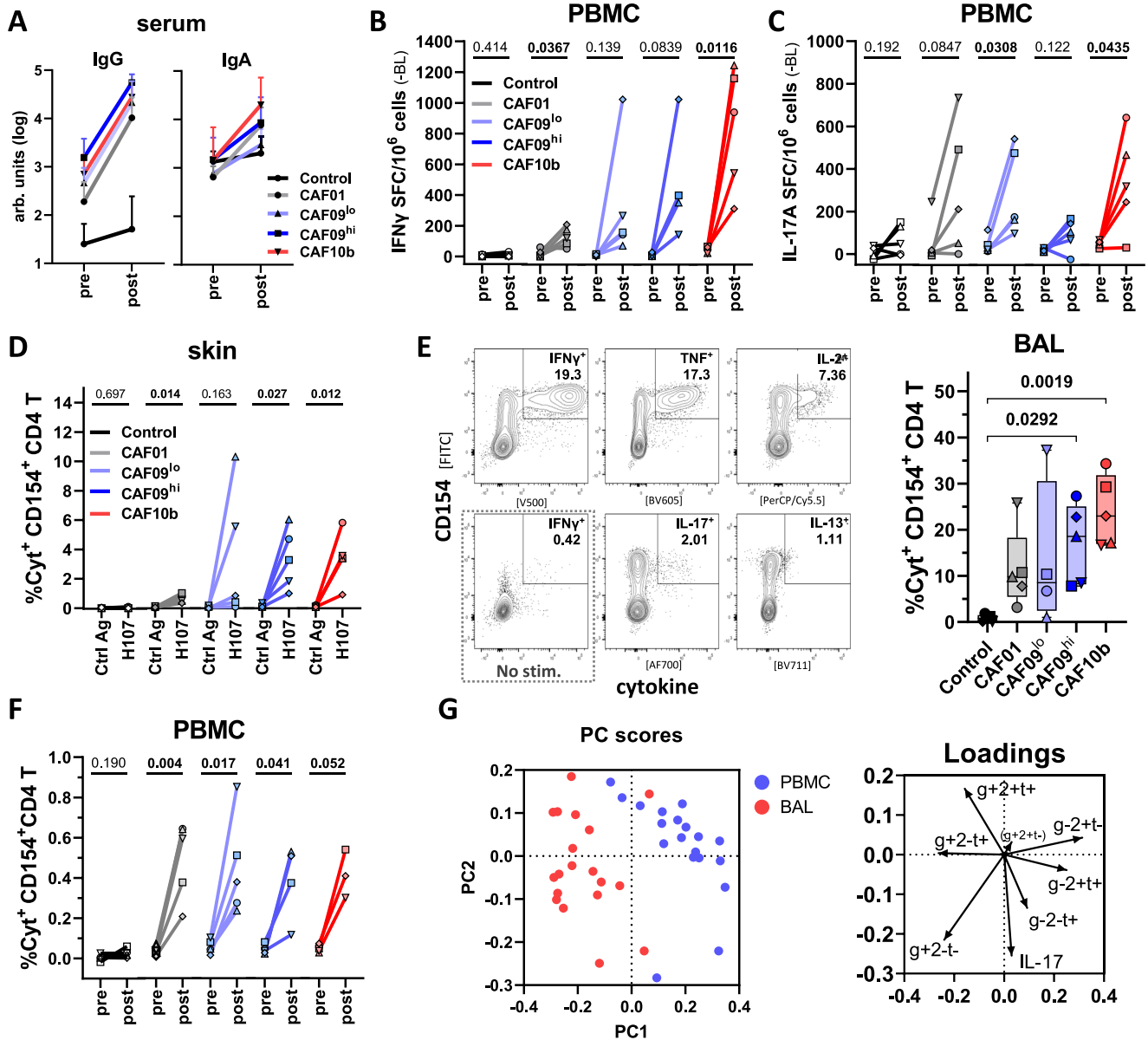


Fig. 7 | In vivo antigen delivery recalls local and systemic memory responses.

Six months after the final immunization, non-human primates were given an in vivo antigen recall in the skin and lungs with H107, or a control protein, as shown in (Fig. 6). **A** Serum H107-specific IgG (left) and IgA (right) antibody levels as measured by ELISA before (pre) and post in vivo antigen recall of H107/CAF[®]-immunized Non-human primates. Symbols represent mean ± SD of arbitrary units, *n* = 5/grp. **B, C** PBMCs from control and H107/CAF[®]-immunized NHPs (*n* = 5/grp) were assessed by ELISpot assay pre- and post in vivo antigen recall. PBMCs were stimulated ex vivo for H107-specific (**B**) IFN γ and (**C**) IL-17A production as in Fig. 5. **D** The percentage of CD4 T cells isolated from skin biopsies collected from control antigen (Ctrl Ag) and H107 protein ID injection sites that express IFN γ , TNF, IL-2, IL-17, and/or IL-13 after ex vivo stimulation with H107 protein, as assessed by intracellular cytokine staining (ICS), *n* = 5/grp. **E** Sample contour plots of ICS analysis of CD4 T cells isolated from

the BAL of a representative H107/CAF[®]10b-immunized animal 8 days after in vivo antigen (left), and the resultant summary data of the total % H107-specific cytokine-expressing BAL CD4 T cells. Bars represent median ± IQR, min. and max. Symbols, individual animals, *n* = 5/grp, *n* = 4 CAF[®]09^o. *P* values, two-sided Mann-Whitney *U* tests. Kruskal-Wallis test *p* = 0.0097. **F** The percentage of cytokine-producing CD4 T cells from PBMC samples collected pre- and post in vivo antigen recall assessed IFN γ , TNF, IL-2, IL-17, and/or IL-13 after ex vivo stimulation with H107 protein. **B–D, F** Symbols and lines, individual animals *n* = 5/grp. *P* values within groups from two-sided paired *T* test. **G** Principle component analysis (PCA) of H107-specific CD4 T cells from BAL (red) and PBMC (blue) for IL-17 and combinatorial IFN γ /TNF/IL-2 expression. PC1 and PC2 loading axes shown. Symbol, individual H107/CAF[®]-immunized animals, *n* = 5/grp. Source data are provided as a Source Data file.

of skin biopsy-derived cells followed by intracellular cytokine staining (ICS) for production of IFN γ , TNF, IL-2, IL-17, and/or IL-13 (Fig. 7D) showed a specific recruitment of H107-specific CD4 T cells to the H107 injection site for all vaccine groups, with the highest frequency of H107-specific CD4 T cells found in the H107/CAF[®]09^{hi} and H107/CAF[®]10b cohorts (Fig. 7D and S8B, for ICS gating strategy see Figs. S8A and 7E). Local pulmonary recall was also assessed by ICS of BAL cells collected from the right lung eight days after antigen

instillation. Here as well, prominent CD4 T cell recall was found in all immunized groups, with the percentage of H107-specific CD4 T cells highest for those previously immunized with H107/CAF[®]10b (Fig. 7E). Upon H107 restimulation ex vivo, the primary CD4 T cell-produced cytokines observed in the BAL, were the Th1 cytokines IFN γ , TNF and IL-2, with a notable population of IL-17-producing Th17 cells and a lesser population producing IL-13 (Fig. 7E, S8C). H107-specific CD4 T cells were expanded in the blood of all CAF[®]-immunized animals

(Fig. 7F, S8D). Notably, H107-specific cytokine production was not observed for CD8 T cells in the skin, BAL, or PBMC (Fig. S8E–H), supporting that the antigen-specific CMI responses induced by these H107/CAF[®] vaccines and measured by ELISpot and ICS represented Th1/Th17 CD4 T cellular responses (Fig. 6B–F). We found no significant correlation between H107-specific responses in the blood prior to antigen recall (wk30, Fig. 7F pre) and subsequent CD4 T cell responses in the BAL (Fig. 7E), suggesting that the systemic CD4 T cell memory may not predict in vivo recall in the lung (Fig. S8I). Instead, there was a positive correlation between H107-specific CD4 T cells in the blood and BAL *after* recall ($r = 0.5748, p = 0.013$, Fig. S8I), indicating that local and systemic recall responses are related. Finally, principle component analysis (PCA) of a combinatorial Boolean cytokine expression profiles of these post-recall H107-specific CD4 T cells, demonstrated a site-specific phenotypic distinction between PBMCs and BAL (Fig. 7G). The antigen-specific CD4 T cell in the blood were differentiated by TNF + IL-2+ and IL-2+ expression, while the BAL cells were characterized by IFN γ + and IFN γ + TNF + CD4 T cells (Fig. 7G) that reflected an effector/effector memory phenotype⁴⁶.

In summary, the in vivo antigen administration 6 months after immunization induced robust systemic and local CMI and antibody recall responses across all adjuvants at the sites of instillation, demonstrating feasibility of the approach to assess functional memory. Overall, CAF[®]10b displayed the highest CMI recall responses with significant expansion of both Th1 and Th17 cells.

Discussion

Difficult-to-target diseases, for which conventional approaches are incomplete or have failed, pose special challenges to vaccine design. Thus, development of improved vaccines against such targets likely depends on vaccine platforms with diverse immune signatures. Since the delineation of Th1 and Th2 cells in the 1980s⁴⁷, several other T cell subsets have been identified, including Th17 cells that were described in 2005^{48,49}. Now, almost two decades later, current licensed adjuvants induce antibodies, Th1 and Th2 cells, but not Th17 cells, despite their implication in protection against major diseases and pathogens including influenza^{10,12}, chlamydia⁵⁰, *Klebsiella pneumoniae*⁵¹, group A streptococci^{52,53} and tuberculosis^{5,54}. Notably, in experimental settings, immunizations that do induce Th17 responses have been limited to mucosal delivery, including live viral vectored vaccines and BCG (Bacillus Calmette Guérin)^{7,13,14,55}. With the goal of closing this gap, our comparative studies demonstrate the value of head-to-head adjuvant studies and identifies CAF[®]10b as a new liposomal adjuvant that induces strong immune responses in both mice and NHPs with robust Th1/Th17 memory after intramuscular injection.

Inspired by data from the mouse model²⁹, we initiated our search for an improved adjuvant for human use, ultimately assessing the potential of CpG2006 as an add-on to the CAF[®] platform¹⁷. Consistent with previous results^{29,56}, we confirmed that CpG2006 activates human TLR9, as well as murine TLR9, and that highly stable CAF[®]10b liposomes could be formed by formulating CpG2006 with DDA/MMG (Fig. 1). Although not able to induce Th17 cells alone, CpG2006 within CAF[®]10b liposomes increased the CAF[®]-driven Th1/Th17 responses in mice, while simultaneously reducing the systemic inflammatory effects of CpG2006 alone (Fig. 1). When combined with the TB vaccine antigen H107²⁵, this CAF[®]10b-induced Th1/Th17 phenotype was associated with increased protection against murine Mtb challenge, compared to CAF[®]09 formulations^{28,33} that induced significantly lower Th17 responses (Fig. 2). While this demonstrates the functional capacity of CAF[®]10b-induced immunity to protect against an airway pathogen, it also adds to the accumulating support for a protective role of combined Th1/Th17 responses against TB^{5,7,14,25,54,55}.

To better assess the translational potential of CAF[®]10b for human use, we turned to the NHP model and compared the specific humoral and cellular responses to previous CAF[®] formulations, CAF[®]01 and

CAF[®]09, which already have clinical and NHP data for comparison. Here we observed that two intramuscular injections with H107/CAF[®]10b led to serum IgG responses that were sustained at approximately 2-fold (0.323 log) higher than for CAF[®]01 (Fig. 4). This is remarkable, as CAF[®]01 has already been shown to induce 5–6 fold higher IgG titers than alum in a head-to-head clinical trial¹⁹. In addition, we also observed induction of serum IgA responses, which could be important for certain viral targets, including SARS-CoV-2 for which serum IgA has shown superior capacity to neutralize^{57,58}.

While antibodies play an important role in immunity against many pathogens, control of some disease targets benefit from, or even require, a potent CMI response. These include bacterial and viral diseases like chlamydia⁵⁹, TB²⁶, COVID-19⁶⁰, RSV^{61,62}, and influenza⁶³ where effective pathogen control is associated with a Th1 phenotype, in contrast to Th2 cells that associate with disease severity^{60,63–66}. We were therefore intrigued to find that CAF[®]10b induced an increased Th1 memory response that was detectable in circulation six months after intramuscular injection (Fig. 5). Interestingly, CAF[®]09^{hi} initially induced slightly higher peak Th1 responses, but after six months, this had contracted to baseline levels, highlighting that peak responses do not necessarily predict systemic memory. This is conflicting with models where the cellular memory pool is formed as a subset of the effector response, which has been described for effector memory CD4 T cells⁶⁷ and memory CD8 T cells^{68,69}. However, central memory CD4 T cells are generated as an independent subpopulation of the effector response⁶⁷ and the discrepancy between peak and memory responses could therefore be explained by differential imprinting of the central memory T cell pool. Although our study was not designed to differentiate such models, our findings do stress the importance of performing long-term experiments to assess and compare vaccine ability to induce true memory responses.

In addition to Th1 cells, we also found Th17 responses in NHPs vaccinated with CAF[®]01, CAF[®]09^{lo} and CAF[®]10b (Fig. 5). Notably, the IL-17 response for CAF[®]10b was still detectable at termination of the study, 26 weeks after the last immunization, which is consistent with previous data from the mouse model showing that vaccine-induced Th17 cells are maintained as a phenotypically stable subset⁷⁰. To our knowledge, this is the first report of robust adjuvant-induced Th17 responses in NHPs after intramuscular administration.

Notably, we did not detect a Th17 response for CAF[®]09^{hi} in NHPs. CAF[®] liposomes containing either TDB or MMG drive Th1/Th17 responses via stimulation of the C-type lectin receptor Mincle, which leads to induction of proinflammatory cytokines like IL-1 β , IL-6, TNF and TGF- β ¹⁷. In contrast, poly(I:C) agonism of TLR3 drives type I IFN responses⁴⁴, which have been shown to suppress Th17 responses in autoimmune and bacterial infection settings^{41–43}. In this study we also observed that CAF[®]09 activated IRF in human THP-1 reporter cells in a poly(I:C) dose dependent manner (CAF[®]09^{hi} > CAF[®]09^{lo}), whereas CAF[®]01 and CAF[®]10b had no IRF induction (Fig. 5). Moreover, gene expression analysis of whole blood samples taken one day after the first immunization in NHPs demonstrated that type I IFN pathways were more highly upregulated after CAF[®]09^{hi} versus CAF[®]10b immunization, which is consistent with a recent report showing that CAF[®]09 administration drives expression of type-I IFN related genes in mice⁷¹. Although the CAF[®]09^{hi} formulation also induced other proinflammatory pathways, including IL-1, IL-6, and TNF, it is intriguing to consider that TLR3-driven Type I IFNs are related to the observed reduction in Th17 responses across mice and NHPs, which should be further investigated.

Head-to-head studies are costly to perform and consequently, most studies are performed in mice. In this study we conducted head-to-head experiments in both mice and NHPs, observing notable differences in the hierarchies of the adjuvant-mediated adaptive immune responses. For example, while the Th1/Th17 responses induced by CAF[®]01 were relatively greater than those induced by CAF[®]09^{lo/hi} in

mice (Fig. 2), this was not so in NHPs (Fig. 5). Similarly, CAF[®]09 has previously been shown to induce greater cellular and humoral responses than CAF[®]01 in cattle⁷². These species-specific differences could in part be driven by differential expression of pattern recognition receptors and/or differential sensitivity to different immunostimulants, as has been reported for Mincle-ligands⁷³ and various CpGs⁷⁴. Therefore, even though we observed that some aspects of the adjuvant responses were consistent across mice and NHPs (e.g. the diminished Th17 responses of CAF[®]09 formulations), the species-specificity of our data underscores the importance of broad species testing of vaccines in preclinical settings and when evaluating candidates for further clinical development.

While peripheral blood samples are often used to characterize memory responses, effective immunological memory requires enhanced responses to antigen re-exposure in the relevant tissues. As an approach to studying such local memory responses, we applied a sterile in vivo antigenic challenge model to investigate recall into the skin and lungs of NHPs six months after vaccination (Fig. 6). Here we observed significant recall responses both locally and systemically, including presence of antigen-specific IgG in the lungs (BAL) and increased IgG responses in the serum for all CAF[®] adjuvants tested (Fig. 7). Blood CMI responses were also recalled, including Th17 cells, which may be underrepresented in blood samples^{38,39}. Local CMI responses were specifically recruited to H107-injected skin sites, and H107-specific CD4 T cells were found in the BAL of animals across the immunization groups. The striking local and systemic expansion of Th17 cells, as measured by both ELISpot and flow cytometry, is in line with mouse data for CAF[®]01 wherein parenteral vaccination leads to a small pool of Th17 cells that significantly expand in response to mucosal infection by either vaginal *Chlamydia trachomatis*⁵⁰ or aerosol Mtb⁷⁵. In general, the observed relative hierarchy of the measured responses (IgG, Th1, Th17) amongst adjuvants in these studies was retained following antigen recall, with the highest systemic and local CMI responses in the CAF[®]10b-adjuvanted group.

In this study, with the limitation of not providing insights into disease-specific protective immunity of a classical challenge model, the in vivo antigenic recall approach was found to be a highly sensitive method to amplify CMI memory responses otherwise not detectable in the blood. For example, recalled CD4 T cell responses were evident for CAF[®]01 and CAF[®]09-immunized animals, even though such CMI responses were undetectable in the blood prior to recall (Fig. 7). This is consistent with evidence that the majority of memory T cells may reside within the tissues and not in circulation⁷⁶, and that CAF[®]01 itself has been shown to induce both T_{CM} and lung-localized T_{RM} even after parenteral immunization^{70,77,78}. Our data thus demonstrate the potential of utilizing in vivo recall approaches in clinical development to better assess vaccine performance. Skin recall, as demonstrated here, may represent a relatively low-invasive approach evaluate vaccine-induced memory persistence, while airway recall represents an approach to study vaccine potential where mucosal responses are desired. Therefore, we were intrigued to see that the inflammation induced by our pulmonary antigen recall of CAF[®]10b-immunized NHP was highly localized and short-lived (<7 days) (Fig. 6). Future studies in humans could focus on lung sampling, similar to experimental studies with pulmonary delivery of BCG^{79,80}, or sampling of the upper airway mucosa, as has recently been used to study local responses to SARS-CoV-2⁸¹.

Overall, our comparative studies of established and novel CAF[®] formulations identified CAF[®]10b as an adjuvant formulation able to drive true memory antibody, Th1, and Th17 vaccine-responses via a non-mucosal immunization route and across both rodent and primate species. Given these results and the potential to fill an unmet gap in the existing pipeline of vaccine adjuvants, a first in human Ia/Ib trial with CAF[®]10b has been initiated, which includes local antigen recall in the upper airways (NCT06050356).

Methods

Antigen and adjuvant production and characterization

The H107 fusion protein²⁵ is composed of eight Mtb antigens, of which ESAT-6 is repeated four times: PPE68-[ESAT-6]-EspI-[ESAT-6]-EspC-[ESAT-6]-EspA-[ESAT-6]-MPT64-MPT70-MPT83. Recombinant H107 protein was produced and purified as in accordance with established methods²⁵. Briefly, the DNA construct was codon-optimized for expression in *E. coli* and inserted into the pJ411 expression vector (ATUM, Menlo Park, CA, US). H107 contained a His-tag at the N-terminal end (MHHHHHH-). After transformation into *E. coli* BL21 (DE3) (Agilent, DK), protein expression was induced with 1 mM isopropyl β-D-1-thiogalactopyranoside in 3-liter cultures, and the H107 protein was purified from inclusion bodies by metal chelate chromatography followed by anion-exchange chromatography. The H56 fusion protein²⁷ (composed of three Mtb antigens: Ag85B, ESAT-6, and Rv2660) and the control recall protein CTH522⁴⁵ (composed of *Chlamydia trachomatis*-specific antigens) were produced and supplied by Vaccine Development at Statens Serum Institut according to good manufacturing practice (GMP)¹⁹. All protein preparations were sterile filtered and dialyzed into 20 mM Glycine, pH9.2.

Liposomal adjuvants CAF[®]01 and CAF[®]09^{lo} (CAF[®]09b) were prepared by adding aqueous buffer to DDA-TDB or DDA-MMG lipid powder followed by heating and high shear mixing. For CAF[®]09^{lo} Poly(I:C) was subsequently added.⁸² CAF09^{hi} was produced by dissolving DDA and MMG-1 in 99% (v/v) EtOH. The formulations were dried under N₂ for 2 h, followed by air-drying overnight. The dry lipid films were rehydrated in Tris buffer by high-shear mixing (HSM) at 60 °C. The poly(I:C) was added continuously during HSM using a peristaltic pump. CAF09^{hi} contains double concentration of MMG and Poly(I:C) compared to CAF09^{lo}. CAF[®]10b was produced analogously to CAF09^{hi}, by incorporating CpG ODN 2006 (InVivoGen or BionScience, Gera, Germany) with the sequence 5'-tcgtcgtttgtcgtttgtcgtt-3' into DDA/MMG liposomes²⁹.

Adjuvants were characterized for particle size and polydispersity index (PDI) by dynamic light scattering (photon correlation spectroscopy technique). Surface charge was analyzed by measuring the zeta potential (laser-Doppler electrophoresis). For the size measurements, the samples were diluted 10 times, whereas for the zeta potential measurements, the samples were diluted 100 times in milli-Q water. The measurements were performed at 25 °C by using a Zetasizer Nano ZS (Malvern Instruments, Worcestershire, UK) equipped with a 633 nm laser and 173° detection optics. Malvern DTS v.6.20 software was used for data acquisition and analysis. DDA and MMG content was measured by HPLC using an Ultimate 3000 HPLC with a Corona Veo Charged Aerosol Detector (Thermo Fisher Scientific, Waltham, MA, USA). Chromeleon software version 7.2 SR5 was used for data acquisition and analysis. CpG content was measured in a 96 well plate using Ribogreen[™] fluorescence staining kit from Thermo Fisher and a SpectraMax i3 plate reader (Molecular devices, San Jose, CA, USA). CpG content was measured in a 96 well plate using Ribogreen[™] fluorescence staining kit from Thermo Fisher and a SpectraMax i3 plate reader (Molecular devices, San Jose, CA, USA). Differential Scanning Calorimetry Analysis of the liposomes was determined using a MicroCal PEAQ-DSC version 1.61 (Malvern Panalytical Nordic AB, Naerum, Denmark) for data acquisition and analysis. Stability was measured for up to 12 months.

TLR9 activation assay

HEK-Blue[™] hTLR9 and HEK-Blue[™] mTLR9 cells (InVivoGen, USA) were grown under selection media at 37 °C according to manufacturer's instruction. Cells were seeded into 96-well flat bottom plate and stimulated in vitro with decreasing concentrations (100, 10, 1 μg/ml) of CpG2006 or CpG1826 for 17 hrs at 37 °C. Supernatants were collected and assayed for SEAP activity using HEK-Blue detection QUANTI-Blue[™]

(InvivoGen, USA) as per manufacturer instructions. Assays were read using a SpectraMax iD3 (Molecular Devices).

Mouse studies

Mouse. Six-to-eight week old female CB6F1/OlaHsd (H2^{b,d}) mice were obtained from Envigo (Netherlands). Mice were randomly assigned to cages upon arrival and acclimatized at least one week to the animal facility. During the course of the experiment, mice had access to irradiated Teklad Global 16% Protein Rodent Diet (Envigo, 2916 C) and water ad libitum. Mice were housed under Biosafety Level (BSL) II or III conditions in individually ventilated cages (Scanbur, Denmark) in the animal facilities at Statens Serum Institut and maintained in rooms with controlled environment (20–23 °C; relative humidity 55 ± 10%; 12/12 hr light/dark cycle) and had access to nesting material (enviro-dri and soft paper wool; Brogaarden, Denmark) as well as enrichment (aspen bricks, paper house, corn, seeds, and nuts; Brogaarden). Statens Serum Institut's Animal Care and Use Committee approved all experimental procedures and protocols. All experiments were conducted in accordance with the regulations put forward by the Danish Ministry of Justice and Animal Protection Committee under license permit no. 2019-15-0201-00309 and in compliance with the European Union Directive 2010/63 EU.

Immunizations. Mice were immunized subcutaneously (SC) two times with three-week intervals in a volume of 200 µl or 50 µl, respectively. Recombinant antigen was diluted in Tris-HCL buffer + 2% glycerol (pH 7.2) to a concentration of 2 µg and formulated in CCAF[®]01 (250/50 µg DDA/TDB), CAF[®]10b(250/50/20 µg DDA/MMG/CpG2006), CAF[®]09^o (250/50/12.5 µg DDA/MMG/poly(I:C)), or CAF[®]09^{hi} (250/100/25 µg DDA/MMG/poly(I:C)). For BCG immunization, a SC injection of 5 × 10⁵ CFU BCG-Danish aligned with the first H107 immunization.

Preparation of single-cell suspensions. Spleens were aseptically harvested from euthanized mice and forced through 70-µm cell strainers (BD) with the plunger from a 3 mL syringe (BD). Cells were washed twice in cold RPMI or PBS followed by 5 minutes centrifugation at 700 × g. Cells were finally resuspended in supplemented RPMI medium containing 10% fetal calf serum (FCS) (34). Cells were counted using an automatic Nucleocounter (Chemotec) and cell suspensions were adjusted to 2 × 10⁵ cells/well for ELISA and 1–2 × 10⁶ cells/well for flow cytometry. and serum collection.

Cytokine ELISAs. Splenocytes were cultured in the presence of 2 µg/mL recombinant protein antigen for 3 days at 37 °C. Supernatants were harvested and analyzed for levels of IFNγ and IL-17A using enzyme-linked immuno-sorbent assay (ELISA)⁷⁰. Microtiter plates (96-well; Maxisorb; Nunc) were coated with 1 µg/mL capture antibodies (IFNγ: clone R4-6A2, BD Pharmingen; or IL-17A: clone TC11-18H10.1, BioLegend) diluted in carbonate buffer. Free binding sites were blocked with 2% (w/v) skimmed milk powder (Natur Drogeriet, Matas, Denmark) in PBS. Culture supernatants were diluted in PBS with 2% Bovine Serum Albumin (BSA, Sigma-Aldrich) incubated overnight in plates. IFNγ was subsequently detected using a 0.1 µg/mL biotinylated rat anti-murine Ab (clone XMGL2; BD Pharmingen) and recombinant IFNγ (BD Pharmingen) as a standard. IL-17A was detected using 0.25 µg/mL biotinylated anti-mouse IL-17A (BioLegend, clone: TC11-8H4) and recombinant IL-17A (BioLegend). Streptavidin HRP (BD Pharmingen, CA, US) diluted 1:5000 in PBS 1% BSA was used to detect bound biotinylated detection antibodies. The enzyme reaction was developed with 3,3',5,5'-tetramethylbenzidine, hydrogen peroxide (TMB Plus; Kementec), stopped with 0.2 M H₂SO₄ solution and plates read at 450 nm with 620 nm background correction using an ELISA reader (Tecan Sunrise).

Intracellular cytokine staining (ICS). Splenocytes stimulated ex vivo with 2 µg/mL H107 protein antigen in the presence of 1 µg/mL anti-

CD28 (clone 37.51) and anti-CD49d (clone 9C10-MFR4.B) for 1 hour at 37 °C, 5% CO₂ followed by the addition of Brefeldin A to 10 µg/mL (Sigma Aldrich; B7651-5mg) and 5 hours of additional incubation at 37 °C, after which the cells were kept at 4 °C until staining. Cells were stained with surface markers diluted in 50% brilliant stain buffer (BD Horizon; 566349) using anti-CD4-BV510, anti-CD8-PerCP-Cy5.5, anti-CD44-BV786 at 4 °C for 20 min, before fixation and permeabilization using the Cytofix/Cytoperm kit (BD Biosciences) as per manufacturer's instructions, followed by intracellular staining for anti-CD3-BV650, anti-IFNγ-PE-Cy7, anti-IL-2-APC-Cy7, anti-TNF-PE, anti-IL17-BV421. Cells were characterized using a BD LSRFortessa and the FSC files were manually gated with FlowJo v10 (TreeStar). Non-stimulated cells were used to set gate boundaries for cytokine markers.

Serum collection and assays. Blood was collected via cardiac puncture and serum isolated by centrifugation.

H107-specific antibody detection was performed by ELISA. Maxisorb Plates (Nunc) were coated overnight at 4 °C with H107 (0.1 µg/ml) and then blocked for with 2% BSA in PBS for 2 hrs at room temperature. Sera were diluted 30X followed by three-fold serial dilutions and incubated 2hr at room temperature 4 °C on plates. Total IgG was detected with horse radish peroxidase (HRP)-conjugated goat anti-mouse IgG (Invitrogen) diluted 1:32,000. IgG1 was detected with HRP-conjugated goat anti-mouse IgG1 (Southern Biotech) diluted 1:16,000. IgG2c was detected with HRP-conjugated rabbit anti-mouse IgG2c (Southern Biotech) diluted 1:5000. The enzyme reaction was developed with 3,3',5,5'-tetramethylbenzidine, hydrogen peroxide (TMB Plus; Kementec), stopped with 0.2 M H₂SO₄ solution and plates read at 450 nm with 620 nm background correction using an ELISA reader (Tecan Sunrise).

The Mouse U-plex kit for the cytokines IL-12p70, IL-6, TNF, MCP-1 was performed according to the manufacturer's instructions (Meso Scale Discovery) to measure cytokine concentrations in serum. The plates were read on the Sector Imager 2400 system (Meso Scale Discovery) and calculation of cytokine concentrations in unknown samples was determined by 4-parameter logistic non-linear regression analysis of the standard curve.

Aerosol infection and bacterial counting. Ten weeks after the first immunization, mice were challenged with Mtb Erdman (ATCC 35801/TMC107). Mtb Erdman was cultured in Difco™ Middlebrook 7H9 (BD) supplemented with 10% BBL™ Middlebrook ADC Enrichment (BD) for two-three weeks using an orbital shaker (-110 rpm, 37 °C). Bacteria were harvested in log phase and stored at -80 °C until use. Bacterial stocks were thawed, sonicated for five minutes, resuspended with a 27 G needle, and mixed with PBS to the desired inoculum dose. Using a Biaera exposure system controlled via AeroMP software, mice were challenged by the aerosol route with virulent Mtb Erdman in a dose equivalent to 50-100 CFUs. To determine vaccine efficacy, Mtb CFU were enumerated in lungs of aerosol infected mice. Left lung lobes were homogenized in 3 mL MilliQ water containing PANTA™ Antibiotic Mixture (BD, cat.no. #245114) using GentleMACS M-tubes (Miltenyi Biotec). Lymph nodes were forced through 70-µm cell strainers (BD Biosciences) in 1 mL PANTA solution. Tissue homogenates were serially diluted, plated onto 7H11 plates (BD), and grown for 14 days at 37 °C and 5% CO₂. CFU data were log-transformed before analyses.

Non-Human Primate (NHP) studies

NHPs. Cynomolgus macaques (*Macaca fascicularis*), aged 27-30 months (16 females and 14 males) and originating from Mauritian AAALAC certified breeding centers, were used in this study. All animals were housed in IDMIT facilities (CEA, Fontenay-aux-roses) under BSL-2 containment (Animal facility authorization #D92-032-02, Préfecture des Hauts de Seine, France) and in compliance with European Directive 2010/63/EU, the French regulations and the Standards for Human Care

and Use of Laboratory Animals, of the Office for Laboratory Animal Welfare (OLAW, assurance number #A5826-01, US). The protocols were approved by the institutional ethical committee Comité d'Éthique en Expérimentation Animale du Commissariat à l'Énergie Atomique et aux Énergies Alternatives (CÉTEA no. 44) under statement number A19_027. The study was authorized by the Research, Innovation and Education Ministry under registration number APAFIS #720-201505281237660 v3.

NHP Immunizations and sampling. The 25 *Cynomolgus* macaques were randomly divided into five experimental groups with 5 animals in each. The different vaccine prime-boost regimens for the five groups are illustrated in Fig. 3. Animals were sedated with ketamine hydrochloride and medetomidine hydrochloride (10 mg/kg body weight intramuscularly). H107 (20 µg per animal) was administered by the intramuscular (IM) route into the right thigh with adjuvant CAF®01 (625/125 µg DDA/TDB), CAF®10b(625/125/50 µg DDA/MMG/CpG2006), CAF®09^{lo} (1250/250/62.5 µg DDA/MMG/poly(I:C)), or CAF®09^{hi} (1250/500/125 µg DDA/MMG/poly(I:C)) in 10 mM Tris + 4% glycerol, pH 7.0 to a total volume of 0.5 mL, at weeks 0 and 4. Control animals received 0.5 mL phosphate buffered saline, pH 7.0. All animals were sampled for blood 2 weeks before the first vaccination and at weeks 0, 2, 4, 6, 8, 10, 12 and 30 (Fig. 3).

In vivo antigen recall in NHPs. During the antigen recall part of the study, six months post the final immunization (see Fig. 3), Purified H107 protein (50 µg per animal in 0.15 mL) was administered by intratracheal route (IT) using endoscope, directly inserted into the trachea until the bifurcation of caudal right lung (accessory lobe and caudal lobe). In parallel, purified H107 and control protein antigen (CTH522; composed of unrelated *Chlamydia trachomatis*-specific antigens) were administered by intradermal (ID) route consisted of two intradermal injections of 0.1 mL, each containing 20 µg protein antigen per injection the right (H107) or left (control antigen) side of the back of the animal. In vivo recall antigens were diluted in 10 mM Tris + 4% glycerol, pH 7.0. Pre-medication was performed using alpha-2 agonist atropine sulfate (0.04 mg/kg) before anesthesia of the animals to reduce bronchospasm and mucus production during endoscopic exam. Animals were then sedated using ketamine hydrochloride (5 mg/kg, IM) associated with medetomidine hydrochloride (0.05 mg/kg IM). After bronchoscopy administration and sampling, animals are injected with Atipamezol hydrochloride (0.25 mg/kg) to induce recovery from anesthesia. The animals were sampled for blood at days 0, 3 and 8. On day 8, bronchoalveolar lavage (BAL) was also performed using 50 mL sterile saline, and skin biopsy were performed at injection sites. Blood cell counts, hemoglobin and hematocrit were determined from EDTA-treated blood using an HMX A/L analyzer (Beckman Coulter).

Dermal scoring (skin induration, DTH) was performed at days 0 and 8 post boost. Dermal scoring of the dosing site included observations and graded scoring for erythema, edema, bleeding, scabbing, fissuring and/or ulceration. Skin biopsies were gathered using 8mm² punches and put in PBS after fatty tissue was removed. Briefly, skin biopsies were washed using RPMI 37 °C and incubated overnight at 37 °C in enzymatic solution (RPMI Glutamax+ 5%FCS+ 1%ATB+DNase 0.02 mg/L) with 4 mg/mL Collagenase D. After incubation, supernatant was collected, aliquoted, and stored at -80 °C for antibody ELISA assays. The remaining tissue was dissociated and washed before harvesting cells for stimulation for ICS assays.

ELISpot assays. Fresh PBMCs were used for ex vivo stimulation with purified H107 protein or a pool of overlapping 15-mer peptide with (5-10 amino acid overlap) spanning the H107 antigen²⁵ for ELISpot analysis. Briefly, Monkey IFN γ ELISpot PRO kit (Mabtech, Cat #3421M-2APT, Nacka, Sweden) and Monkey IL17A ELISpotPLUS Kit (Mabtech,

Cat #3520M-4APW-10) were used following manufacturer's instructions with 2×10^5 freshly isolated PBMC added to each well. For IL-17A, H107 protein (5 µg/mL) was added in duplicate in the culture medium, and plates incubated -40 hr at +37 °C in 5% CO₂ atmosphere. For IFN γ , in order to reduce nonspecific background that was initially observed in pre-immunization screenings, the H107 peptide pool (2 µg/mL of each peptide) was used for overnight (-18 hr) H107-specific stimulation. Culture medium was used as negative control, and PMA/ionomycin stimulation as a positive control. Plates were then washed 5 times with PBS, followed by addition of biotinylated anti-IFN γ or anti-IL-17A antibodies and a 2 h incubation at 37 °C. Plates were washed 5 times with PBS, and spots were developed with NBT/BCIP substrate solution. The spots were counted with an Automated Elispot Reader System ELRO8IFL (Autoimmun Diagnostika GmbH, Strassberg, Germany).

Flow cytometry. Fresh PBMCs, BAL cells and skin cells were isolated and ($1-2 \times 10^6$) were resuspended in 150 µL of complete medium containing 0.2 µg of each costimulatory antibody CD28 and CD49d (FastImmune CD28/CD49d, BD). Stimulation was performed in 96 well/plates using H107 protein (5 µg/mL), ESAT-6 peptide pool (2 µg/mL), H107 peptide pool (1 µg/mL)²⁵ or PMA/Ionomycin (as positive control) or culture medium alone (as negative control). Brefeldin A was added to each well at a final concentration of 10 µg/mL and the plate was incubated at 37 °C, 5% CO₂ overnight. The cells were then washed, stained with a viability dye (dye LIVE/DEAD fixable Blue dead cell stain kit, ThermoFisher), fixed and permeabilized with the BD Cytofix/Cytoperm reagent. Permeabilized PBMCs and BAL cells were stored at -80 °C before the staining procedure. Permeabilized skin samples were directly stained. Staining procedure was performed in a single step following permeabilization using anti-IFN γ (V450, clone B27, BD Biosciences), anti-CD4 (BV510, clone L200, BD Biosciences), anti-TNF (BV605, clone Mab11, BioLegend), anti-IL-13 (BV711, clone JES10-5A2, BD Biosciences), anti-CD154 (FITC, clone REA238, BD Biosciences), anti-IL-2 (PerCP/Cy5.5, clone MQ1-17H12, BD Biosciences), anti-CD8 (PE-Vio770, clone BW135/80, Miltenyi), anti-IL-17A (Alexafluor 700, clone N49-653, BD Biosciences), CD3 (APC-Cy7, clone SP34-2, BD Biosciences). After 30 minutes of incubation at 4 °C in the dark, cells will be washed in BD Perm/Wash buffer. Cells were acquired with an LSR II (BD) after the staining procedure. FlowJo software v10 (TreeStar) was used for sample analysis. PCA analysis was performed using GraphPad Prism v9 software on Boolean gating data normalized to percentage of the total cytokine positive population per individual animal.

PET-CT. Chest PET-CT was performed at baseline prior to antigen recall (D0) and on days 3 (D3) and 7 (D7) post recall. Animals were fasted for at least 8 h before each imaging session. All imaging acquisition was performed using the Digital Photon Counting (DPC) PET-CT system (Vereos-Ingenuity, Philips) implemented in a BSL-3 laboratory. These sessions were always performed in the same experimental conditions (acquisition time and animal order) to limit [18 F]-FDG-PET experimental bias. Animals were first anesthetized with ketamine hydrochloride (5 mg/kg, IM) associated with medetomidine hydrochloride (0.05 mg/kg IM), intubated, and then maintained under 0.5-1.5% isoflurane and placed in a supine position on a warming blanket (Bear Hugger, 3 M) on the machine bed with monitoring of the cardiac rate, oxygen saturation, and body temperature.

Computed Tomography (CT) was performed 5 minutes prior to PET acquisition for attenuation correction and anatomical localization. The CT detector collimation used was 64×0.6 mm, the tube voltage was 120 kV, and the intensity was approximately 150 mAs. Chest-CT images were reconstructed with a slice thickness of 1.25 mm and an interval of 0.63 mm. A whole-body PET scan (3 bed positions, 3 min/bed position) was performed approximately 45 min post-injection of

3.5 ± 0.4 MBq kg⁻¹ of [¹⁸F]-FDG via the saphenous vein. PET images were reconstructed onto a 256 × 256 matrix using OSEM (3 iterations, 15 subsets). After PET acquisition, animals were resuscitated using atipamezole hydrochloride (0.25 mg/kg).

PET images were analyzed using 3DSlicer software (open-source tool). For segmentation, various regions of interest (entire lung and separated lung lobes) were semi-automatically contoured according to anatomical information from CT. A 3D volume of interest (VOI) was interpolated from several ROIs in different image slices to cover each lung lobe excluding background signal (heart and liver). For quantification, [¹⁸F]-FDG accumulation in the VOIs was given as a standardized uptake value (SUV_{mean}, SUV_{max}).

H107-specific antibody ELISAs in NHPs. An indirect quantitative ELISA was developed to measure the content of anti-H107 IgG and IgA antibodies in NHP sera and BAL samples. Maxisorb Plates (Nunc) were coated overnight with purified H107 antigen (0.1 μg/ml) at 4 °C, and then >1.5 hrs blocked with 2% BSA at room temperature. Sera were diluted 1:200 (1:20 from control animals) and thereafter seven 2-fold serial dilutions made. Undiluted BAL and thereafter seven 3-fold serial dilutions were made. Sample dilutions were added to the plates and incubated overnight (-16hrs) at 4 °C. HRP-conjugate anti-IgG (goat anti-Monkey IgG, Fitzgerald Cat# 43R-IG020HRP, at 1:5000 dilution) or IgA (polyclonal rabbit anti-human IgA/HRP, Dako, P0216, at 1:2000 dilution) was added for 1 hr at room temperature and the enzyme reaction was developed with TMB plus (Kementec) for 15 minutes and stopped with 0.2 M H₂SO₄ solution. Plates were read at 450 nm with 620 nm background correction using an ELISA reader (Tecan Sunrise). We confirmed the specificity of our IgA ELISA and non-cross reactivity toward IgG using purified human IgG and IgA (Sigma-Aldrich).

A reference serum pool was established by combining sera from all immunized NHP from study week eight and arbitrarily assigned a value of 10,000 ELISA-Units (arbitrary units). Two-fold serial dilutions of reference sample was run on each plate. For each sample, titers were calculated from five parameter logistic curves based on 2-fold dilution curves using the package drc in R. Sample titer values were based on dilutions from the linear portion of the response curve for IgG and IgA assays. Area under the curve (AUC) calculation was performed in GraphPad Prism v9 after baseline correction.

Expression analyses of whole blood. Whole blood samples collected at baseline before immunizations and 1 day after each immunization were collected into PAXgene® Blood RNA Tubes for gene expression analysis. Total mRNA for each sample was extracted, polyA tail enrichment, and subjected to next generation sequencing by Azenta (Leipzig, Germany). We then processed the raw RNA-seq data by nf-core rnaseq (version 3.12.0)⁸³ a community-curated best practice workflow.

In brief, the sequence read quality was checked by fastqc and the adapter and low-quality reads were trimmed by “Trim Galore!”. The reads were mapped to *Macaca fascicularis* reference genome 6.0 by HISAT2⁸⁴, and annotated by Emsembl 109. The mapped counts were counted by Salmon⁸⁵. Two baseline pre-immunization outlier samples were excluded, based on the distorted distribution of GC% content and the examination of sample PCA (Principal component analysis) plot. The gene expression values of these two outliers were imputed using the group mean of all nonimmunized samples for the downstream analysis. PCA was performed on the top-1500 variable genes. The expression values were normalized to the library size, then log₂-transformed added with pseudo count (+1).

Differential gene expression analysis was performed using DESeq2⁸⁶ (Wald test, two-sided, p-values adjusted by Benjamini–Hochberg method), by separately comparing day 1 after immunization 1 or 2 to the baseline. Genes were identified as differentially expressed by passing the cutoff with the absolute log₂ fold

change > 1, and adjusted p value < 0.05. The differentially expressed gene (DEG) lists were used for pathway enrichment analysis by R-package fgsea⁸⁷. The enrichment scores were calculated using Kolmogorov–Smirnov-like two-tailed test (scoreType = “std”), then normalized to mitigate differences of the gene set size, with p-values adjusted by Benjamini–Hochberg method. The bioinformatics workflow is documented at github.com/INFIMM-Bioinformatics/TB-PAXGENE.

Luciferase assay. THP-1-Dual cells (InVivoGen, USA) were grown under selection media at 37 °C according to manufacturer’s instruction. 10⁵ cells were seeded per well of 96-well flat bottom plate in triplicate and differentiated for 48hrs with PMA (40 ng/ml). PMA was removed and CAF® adjuvants or varying concentrations added to the cells for overnight incubation at 37 °C. Supernatants were collected and secreted Luciferase activity assayed using QUANTI-Luc™ kit (InVivoGen) as per manufacturer instructions. The CyQUANT-LDH-Cytotoxicity assay (Invitrogen) was also performed on supernatants according to manufacturer instructions, confirming that cell viability was not increased compared to untreated cells. Assays were read using a SpectraMax iD3 (Molecular Devices).

Statistics and reproducibility. All Mann-Whitney U and student t tests were performed two-tailed. All statistical tests and PCA analyses were calculated using the statistical Graphpad Prism software v9. No data were excluded from the analyses. Sample sizes for mouse protection studies were chosen via power calculations to detect a treatment effect (protection) of 0.5 log₁₀ CFU reduction in lungs compared to controls with a type I error rate of 5% (α = 0.05), a power of 80% and standard deviation of 0.35 log₁₀ CFU based on previous studies. No statistical method was used to predetermine NHP sample size. The investigators were blinded to allocation during experiments and PET-CT outcome assessment. For other outcomes pre-determined statistical analyses were performed by non-blinded investigators.

Illustrations. Illustrations in Figs. 1B, 1E, 2A, 3, and 6A Created with BioRender.com released under a Creative Commons Attribution-NonCommercial-NoDerivs 4.0 International license.

Reporting summary

Further information on research design is available in the Nature Portfolio Reporting Summary linked to this article.

Data availability

All data associated with this study are present in the paper or the Supplementary Information. The mRNA expression data generated in this study have been deposited in the Gene Expression Omnibus database under accession code [GSE241235](https://www.ncbi.nlm.nih.gov/geo/query/acc.cgi?acc=GSE241235). The flow cytometry data generated in this study have been deposited in the Zenodo data repository under accession code [13332226](https://doi.org/10.5281/zenodo.13332226). Source data are provided with this paper.

References

1. Pulendran, B., S Arunachalam, P. & O’Hagan, D. T. Emerging concepts in the science of vaccine adjuvants. *Nat. Rev. Drug Discov.* **20**, 454–475 (2021).
2. Sarkar, I., Garg, R. & van Drunen Littel-van den Hurk, S. Selection of adjuvants for vaccines targeting specific pathogens. *Expert Rev. Vaccines* **18**, 505–521 (2019).
3. Rodo, M. J. et al. A comparison of antigen-specific T cell responses induced by six novel tuberculosis vaccine candidates. *PLoS Pathog.* **15**, e1007643 (2019).
4. Wilk, M. M. et al. Lung CD4 Tissue-Resident Memory T Cells Mediate Adaptive Immunity Induced by Previous Infection of Mice with *Bordetella pertussis*. *J. Immunol.* **199**, 233–243 (2017).

5. Dijkman, K. et al. Prevention of tuberculosis infection and disease by local BCG in repeatedly exposed rhesus macaques. *Nat. Med* **25**, 255–262 (2019).
6. Monin, L. et al. Immune requirements for protective Th17 recall responses to Mycobacterium tuberculosis challenge. *Mucosal Immunol.* **8**, 1099–1109 (2015).
7. Counoupas, C. et al. Mucosal delivery of a multistage subunit vaccine promotes development of lung-resident memory T cells and affords interleukin-17-dependent protection against pulmonary tuberculosis. *NPJ Vaccines* **5**, 105 (2020).
8. Gideon, H. P. et al. Multimodal profiling of lung granulomas in macaques reveals cellular correlates of tuberculosis control. *Immunity* **55**, 827–846.e810 (2022).
9. Dhume, K. et al. Bona Fide Th17 Cells without Th1 Functional Plasticity Protect against Influenza. *J. Immunol.* **208**, 1998–2007 (2022).
10. Omokanye, A. et al. Clonotypic analysis of protective influenza M2e-specific lung resident Th17 memory cells reveals extensive functional diversity. *Mucosal Immunol.* **15**, 717–729 (2022).
11. Eliasson, D. G. et al. M2e-tetramer-specific memory CD4 T cells are broadly protective against influenza infection. *Mucosal Immunol.* **11**, 273–289 (2018).
12. McKinstry, K. K. et al. IL-10 deficiency unleashes an influenza-specific Th17 response and enhances survival against high-dose challenge. *J. Immunol.* **182**, 7353–7363 (2009).
13. Orr, M. T. et al. Mucosal delivery switches the response to an adjuvanted tuberculosis vaccine from systemic TH1 to tissue-resident TH17 responses without impacting the protective efficacy. *Vaccine* **33**, 6570–6578 (2015).
14. Van Dis, E. et al. STING-Activating Adjuvants Elicit a Th17 Immune Response and Protect against Mycobacterium tuberculosis Infection. *Cell Rep.* **23**, 1435–1447 (2018).
15. Stewart, E. L. et al. Lung IL-17A-Producing CD4+ T Cells Correlate with Protection after Intrapulmonary Vaccination with Differentially Adjuvanted Tuberculosis Vaccines. *Vaccines* **12**, 128 (2024).
16. Enriquez, A. B. et al. Advancing Adjuvants for Mycobacterium tuberculosis Therapeutics. *Front Immunol.* **12**, 740117 (2021).
17. Pedersen, G. K., Andersen, P. & Christensen, D. Immunocorrelates of CAF family adjuvants. *Semin Immunol.* **39**, 4–13 (2018).
18. Schick, J. et al. Cutting Edge: TNF Is Essential for Mycobacteria-Induced MINCLE Expression, Macrophage Activation, and Th17 Adjuvanticity. *J. Immunol.* **205**, 323–328 (2020).
19. Abraham, S. et al. Safety and immunogenicity of the chlamydia vaccine candidate CTH522 adjuvanted with CAF01 liposomes or aluminium hydroxide: a first-in-human, randomised, double-blind, placebo-controlled, phase 1 trial. *Lancet Infect. Dis.* **19**, 1091–1100 (2019).
20. van Dissel, J. T. et al. A novel liposomal adjuvant system, CAF01, promotes long-lived Mycobacterium tuberculosis-specific T-cell responses in human. *Vaccine* **32**, 7098–7107 (2014).
21. Didierlaurent, A. M. et al. Adjuvant system AS01: helping to overcome the challenges of modern vaccines. *Expert Rev. Vaccines* **16**, 55–63 (2017).
22. Tait, D. R. et al. Final Analysis of a Trial of M72/AS01(E) Vaccine to Prevent Tuberculosis. *N. Engl. J. Med* **381**, 2429–2439 (2019).
23. Amezcua Vesely, M. C. et al. Effector T(H)17 Cells Give Rise to Long-Lived T(RM) Cells that Are Essential for an Immediate Response against Bacterial Infection. *Cell* **178**, 1176–1188.e1115 (2019).
24. Christensen, D., Mortensen, R., Rosenkrands, I., Dietrich, J. & Andersen, P. Vaccine-induced Th17 cells are established as resident memory cells in the lung and promote local IgA responses. *Mucosal Immunol.* **10**, 260–270 (2017).
25. Woodworth, J. S. et al. A Mycobacterium tuberculosis-specific subunit vaccine that provides synergistic immunity upon co-administration with Bacillus Calmette-Guérin. *Nat. Commun.* **12**, 6658 (2021).
26. Knudsen, N. P. et al. Different human vaccine adjuvants promote distinct antigen-independent immunological signatures tailored to different pathogens. *Sci. Rep.* **6**, 19570 (2016).
27. Billeskov, R. et al. Testing the H56 Vaccine Delivered in 4 Different Adjuvants as a BCG-Booster in a Non-Human Primate Model of Tuberculosis. *PLoS One* **11**, e0161217 (2016).
28. Mørk, S. K. et al. Personalized therapy with peptide-based neoantigen vaccine (EVX-01) including a novel adjuvant, CAF[®]09b, in patients with metastatic melanoma. *Oncoimmunology* **11**, 2023255 (2022).
29. Karlsen, K. et al. A stable nanoparticulate DDA/MMG formulation acts synergistically with CpG ODN 1826 to enhance the CD4⁺ T-cell response. *Nanomed. (Lond.)* **9**, 2625–2638 (2014).
30. Cooper, C. L. et al. CPG 7909, an Immunostimulatory TLR9 Agonist Oligodeoxynucleotide, as Adjuvant to Engerix-B[®] HBV Vaccine in Healthy Adults: A Double-Blind Phase I/II Study. *J. Clin. Immunol.* **24**, 693–701 (2004).
31. Witzig, T. E. et al. A phase I trial of immunostimulatory CpG 7909 oligodeoxynucleotide and 90 yttrium ibritumomab tiuxetan radioimmunotherapy for relapsed B-cell non-Hodgkin lymphoma. *Am. J. Hematol.* **88**, 589–593 (2013).
32. Volpi, C. et al. High doses of CpG oligodeoxynucleotides stimulate a tolerogenic TLR9–TRIF pathway. *Nat. Commun.* **4**, 1852 (2013).
33. Korsholm, K. S. et al. Induction of CD8⁺ T-cell responses against subunit antigens by the novel cationic liposomal CAF09 adjuvant. *Vaccine* **32**, 3927–3935 (2014).
34. Pitt, J. M. et al. Blockade of IL-10 signaling during bacillus Calmette-Guérin vaccination enhances and sustains Th1, Th17, and innate lymphoid IFN- γ and IL-17 responses and increases protection to Mycobacterium tuberculosis infection. *J. Immunol.* **189**, 4079–4087 (2012).
35. Desel, C. et al. Recombinant BCG Δ ureC hly+ induces superior protection over parental BCG by stimulating a balanced combination of type 1 and type 17 cytokine responses. *J. Infect. Dis.* **204**, 1573–1584 (2011).
36. Darrah, P. A. et al. Boosting BCG with proteins or rAd5 does not enhance protection against tuberculosis in rhesus macaques. *NPJ Vaccines* **4**, 21 (2019).
37. Lorenzen, E. et al. Multi-component prime-boost Chlamydia trachomatis vaccination regimes induce antibody and T cell responses and accelerate clearance of infection in a non-human primate model. *Front Immunol.* **13**, 1057375 (2022).
38. Ogongo, P. et al. Tissue-resident-like CD4⁺ T cells secreting IL-17 control Mycobacterium tuberculosis in the human lung. *J. Clin. Invest* **131**, e142014 (2021).
39. Shanmugasundaram, U. et al. Pulmonary Mycobacterium tuberculosis control associates with CXCR3- and CCR6-expressing antigen-specific Th1 and Th17 cell recruitment. *JCI Insight* **5**, e137858 (2020).
40. Zhang, L., Yuan, S., Cheng, G. & Guo, B. Type I IFN promotes IL-10 production from T cells to suppress Th17 cells and Th17-associated autoimmune inflammation. *PLoS One* **6**, e28432 (2011).
41. Guo, B., Chang, E. Y. & Cheng, G. The type I IFN induction pathway constrains Th17-mediated autoimmune inflammation in mice. *J. Clin. Invest* **118**, 1680–1690 (2008).
42. Shinohara, M. L., Kim, J. H., Garcia, V. A. & Cantor, H. Engagement of the type I interferon receptor on dendritic cells inhibits T helper 17 cell development: role of intracellular osteopontin. *Immunity* **29**, 68–78 (2008).
43. Wu, V. et al. Plasmacytoid dendritic cell-derived IFN α modulates Th17 differentiation during early Bordetella pertussis infection in mice. *Mucosal Immunol.* **9**, 777–786 (2016).
44. Oshiumi, H., Matsumoto, M., Funami, K., Akazawa, T. & Seya, T. TICAM-1, an adaptor molecule that participates in Toll-like receptor 3-mediated interferon- β induction. *Nat. Immunol.* **4**, 161–167 (2003).

45. Olsen, A. W., Follmann, F., Erneholm, K., Rosenkrands, I. & Andersen, P. Protection Against Chlamydia trachomatis Infection and Upper Genital Tract Pathological Changes by Vaccine-Promoted Neutralizing Antibodies Directed to the VD4 of the Major Outer Membrane Protein. *J. Infect. Dis.* **212**, 978–989 (2015).
46. Seder, R. A., Darrah, P. A. & Roederer, M. T-cell quality in memory and protection: implications for vaccine design. *Nat. Rev. Immunol.* **8**, 247–258 (2008).
47. Mosmann, T. R., Cherwinski, H., Bond, M. W., Giedlin, M. A. & Coffman, R. L. Two types of murine helper T cell clone. I. Definition according to profiles of lymphokine activities and secreted proteins. *J. Immunol.* **136**, 2348–2357 (1986).
48. Langrish, C. L. et al. IL-23 drives a pathogenic T cell population that induces autoimmune inflammation. *J. Exp. Med.* **201**, 233–240 (2005).
49. Jiang, S. & Dong, C. A complex issue on CD4(+) T-cell subsets. *Immunol. Rev.* **252**, 5–11 (2013).
50. Nguyen, N. et al. Th1/Th17 T cell Tissue-Resident Immunity Increases Protection, But Is Not Required in a Vaccine Strategy Against Genital Infection With Chlamydia trachomatis. *Front Immunol.* **12**, 790463 (2021).
51. Chen, K. et al. Th17 cells mediate clade-specific, serotype-independent mucosal immunity. *Immunity* **35**, 997–1009 (2011).
52. Wang, B. et al. Induction of TGF- β 1 and TGF- β 2-dependent predominant Th17 differentiation by group A streptococcal infection. *Proc. Natl Acad. Sci. USA* **107**, 5937–5942 (2010).
53. Mortensen, R. et al. Local Th17/IgA immunity correlate with protection against intranasal infection with Streptococcus pyogenes. *PLoS One* **12**, e0175707 (2017).
54. Khader, S. A. et al. IL-23 and IL-17 in the establishment of protective pulmonary CD4+ T cell responses after vaccination and during Mycobacterium tuberculosis challenge. *Nat. Immunol.* **8**, 369–377 (2007).
55. Aguilo, N. et al. Pulmonary but Not Subcutaneous Delivery of BCG Vaccine Confers Protection to Tuberculosis-Susceptible Mice by an Interleukin 17-Dependent Mechanism. *J. Infect. Dis.* **213**, 831–839 (2015).
56. Bauer, S. et al. Human TLR9 confers responsiveness to bacterial DNA via species-specific CpG motif recognition. *Proc. Natl Acad. Sci. USA* **98**, 9237–9242 (2001).
57. Sterlin, D. et al. IgA dominates the early neutralizing antibody response to SARS-CoV-2. *Sci. Transl. Med.* **13**, eabd2223 (2021).
58. Sun, L. et al. Increased in vitro neutralizing activity of SARS-CoV-2 IgA1 dimers compared to monomers and IgG. *Proc. Natl Acad. Sci. USA* **118**, e2107148118 (2021).
59. Gondek, D. C., Olive, A. J., Stary, G. & Starnbach, M. N. CD4+ T cells are necessary and sufficient to confer protection against Chlamydia trachomatis infection in the murine upper genital tract. *J. Immunol.* **189**, 2441–2449 (2012).
60. Tan, A. T. et al. Early induction of functional SARS-CoV-2-specific T cells associates with rapid viral clearance and mild disease in COVID-19 patients. *Cell Rep.* **34**, 108728 (2021).
61. Alwan, W. H., Kozłowska, W. J. & Openshaw, P. J. Distinct types of lung disease caused by functional subsets of antiviral T cells. *J. Exp. Med.* **179**, 81–89 (1994).
62. Tang, Y. W. & Graham, B. S. T cell source of type 1 cytokines determines illness patterns in respiratory syncytial virus-infected mice. *J. Clin. Invest.* **99**, 2183–2191 (1997).
63. Chen, K. & Kolls, J. K. T cell-mediated host immune defenses in the lung. *Annu Rev. Immunol.* **31**, 605–633 (2013).
64. Graham, M. B., Braciale, V. L. & Braciale, T. J. Influenza virus-specific CD4+ T helper type 2 T lymphocytes do not promote recovery from experimental virus infection. *J. Exp. Med.* **180**, 1273–1282 (1994).
65. Ashenafi, S. et al. Progression of clinical tuberculosis is associated with a Th2 immune response signature in combination with elevated levels of SOCS3. *Clin. Immunol.* **151**, 84–99 (2014).
66. Notarbartolo, S. et al. Integrated longitudinal immunophenotypic, transcriptional and repertoire analyses delineate immune responses in COVID-19 patients. *Sci. Immunol.* **6**, eabg5021 (2021).
67. Pepper, M. & Jenkins, M. K. Origins of CD4(+) effector and central memory T cells. *Nat. Immunol.* **12**, 467–471 (2011).
68. Akondy, R. S. et al. Origin and differentiation of human memory CD8 T cells after vaccination. *Nature* **552**, 362–367 (2017).
69. Youngblood, B. et al. Effector CD8 T cells dedifferentiate into long-lived memory cells. *Nature* **552**, 404–409 (2017).
70. Lindenstrøm, T. et al. Vaccine-induced th17 cells are maintained long-term postvaccination as a distinct and phenotypically stable memory subset. *Infect. Immun.* **80**, 3533–3544 (2012).
71. Zimmermann, J. et al. A Novel Prophylaxis Strategy Using Liposomal Vaccine Adjuvant CAF09b Protects against Influenza Virus Disease. *Int J. Mol. Sci.* **23**, 1850 (2022).
72. Thakur, A. et al. Targeting the Mincle and TLR3 receptor using the dual agonist cationic adjuvant formulation 9 (CAF09) induces humoral and polyfunctional memory T cell responses in calves. *PLoS One* **13**, e0201253 (2018).
73. Smith, A. J. et al. Species-Specific Structural Requirements of Alpha-Branched Trehalose Diester Mincle Agonists. *Front Immunol.* **10**, 338 (2019).
74. Roberts, T. L., Sweet, M. J., Hume, D. A. & Stacey, K. J. Cutting edge: species-specific TLR9-mediated recognition of CpG and non-CpG phosphorothioate-modified oligonucleotides. *J. Immunol.* **174**, 605–608 (2005).
75. Lindenstrøm, T. et al. T Cells Primed by Live Mycobacteria Versus a Tuberculosis Subunit Vaccine Exhibit Distinct Functional Properties. *EBioMedicine* **27**, 27–39 (2018).
76. Steinert, E. M. et al. Quantifying Memory CD8 T Cells Reveals Regionalization of Immunosurveillance. *Cell* **161**, 737–749 (2015).
77. Woodworth, J. S. et al. Mucosal boosting of H56:CAF01 immunization promotes lung-localized T cells and an accelerated pulmonary response to Mycobacterium tuberculosis infection without enhancing vaccine protection. *Mucosal Immunol.* **12**, 816–826 (2019).
78. Woodworth, J. S. et al. Subunit vaccine H56/CAF01 induces a population of circulating CD4 T cells that traffic into the Mycobacterium tuberculosis-infected lung. *Mucosal Immunol.* **10**, 555–564 (2017).
79. Davids, M. et al. A Human Lung Challenge Model to Evaluate the Safety and Immunogenicity of PPD and Live Bacillus Calmette-Guérin. *Am. J. Respir. Crit. Care Med.* **201**, 1277–1291 (2020).
80. Morrison, H., Jackson, S. & McShane, H. Controlled human infection models in COVID-19 and tuberculosis: current progress and future challenges. *Front Immunol.* **14**, 1211388 (2023).
81. Roukens, A. H. E. et al. Prolonged activation of nasal immune cell populations and development of tissue-resident SARS-CoV-2-specific CD8(+) T cell responses following COVID-19. *Nat. Immunol.* **23**, 23–32 (2022).
82. Davidsen, J. et al. Characterization of cationic liposomes based on dimethyldioctadecylammonium and synthetic cord factor from M. tuberculosis (trehalose 6,6'-dibehenate)-a novel adjuvant inducing both strong CMI and antibody responses. *Biochim Biophys. Acta* **1718**, 22–31 (2005).
83. Ewels, P. A. et al. The nf-core framework for community-curated bioinformatics pipelines. *Nat. Biotechnol.* **38**, 276–278 (2020).
84. Kim, D., Paggi, J. M., Park, C., Bennett, C. & Salzberg, S. L. Graph-based genome alignment and genotyping with HISAT2 and HISAT-genotype. *Nat. Biotechnol.* **37**, 907–915 (2019).

85. Patro, R., Duggal, G., Love, M. I., Irizarry, R. A. & Kingsford, C. Salmon provides fast and bias-aware quantification of transcript expression. *Nat. Methods* **14**, 417–419 (2017).
86. Love, M. I., Huber, W. & Anders, S. Moderated estimation of fold change and dispersion for RNA-seq data with DESeq2. *Genome Biol.* **15**, 550 (2014).
87. Korotkevich, G. et al. Fast gene set enrichment analysis. Preprint at <https://www.biorxiv.org/content/10.1101/060012v3> (2021).

Acknowledgements

We thank Peter Andersen for his discussions and contribution to study design. We thank Rune Fledelius Jensen for preparation of CAF[®] adjuvants, Vivi Andersen for H107 protein production, and Sara Knudsen for technical support of antibody data analysis. We thank the entire Animal facility staff at SSI for their technical expertise, skills and efforts. We thank the staff of the animal facility of IDMIT, particularly J. Lemaitre, B. Delache, M. Pottier, JM. Robert and Francis Relouzat, the staff of Flow-Cytech laboratory, particularly, M. Gomez-Pacheco, the Immunology and Infectiology teams particularly, L. Bossevot, M. Galpin-Lebreau, M. Leonec and L. Moenne-Loccoz, and R. Marlin, C. Bouillier and I. Mangeot from IDMIT for their technical expertise, skills and efforts. The Infectious Disease Models and Innovative Therapies research infrastructure (IDMIT) is supported by the “Programmes Investissements d’Avenir” (PIA), managed by the ANR under references ANR-11-INBS-0008 (RLG) and ANR-10-EQPX-02-01 (RLG). We thank the Fondation Dormeur Vaduz for the donation of instruments relevant to this project. This work was supported in part by National Institutes of Health/National Institute of Allergy and Infectious Diseases Grant R01AI135721 (RM).

Author contributions

Conceptualization: J.S.W., R.M., D.C., T.L., G.K.P. Methodology: J.S.W., V.C., A.G., T.N., N.B., M.L.O., I.R., R.L.G., T.H., G.K.P., R.M. Resources: D.C., I.R., G.K.W. Investigation: J.S.W., V.C., T.N., N.K., A.G., S.L., E.B., C.J., W.G., J.M., M.L.O., A.S., T.L. Formal Analysis: J.S.W., V.C., T.N., A.G., W.G., G.K.W., T.H., G.K.P., R.M. Visualization: J.S.W., V.C., T.N., A.S., G.K.W., G.K.P., T.H., R.M. Funding acquisition: R.M., F.F. Project administration: J.S.W., V.C., R.L.G., R.M. Supervision: F.F., T.L., R.L.G., G.K.P., R.M. Writing—original draft: J.S.W., R.M. Writing – review & editing: V.C., D.C., T.N., G.K.W., F.F., G.K.P.

Competing interests

JSW, GKP, DC and RM are co-inventors of a patent covering the use of CAF[®]10b and derivatives. All rights have been assigned to Statens

Serum Institut (SSI). DC was employed by SSI during the time of the study, but is now employed by Croda Pharma that, among others, develops and produces immunostimulators, adjuvants and delivery systems for vaccines. The remaining authors declare no competing interests.

Additional information

Supplementary information The online version contains supplementary material available at <https://doi.org/10.1038/s41467-024-52863-9>.

Correspondence and requests for materials should be addressed to Joshua S. Woodworth or Rasmus Mortensen.

Peer review information *Nature Communications* thanks Zhidong Hu and the other, anonymous, reviewer for their contribution to the peer review of this work. A peer review file is available.

Reprints and permissions information is available at <http://www.nature.com/reprints>

Publisher’s note Springer Nature remains neutral with regard to jurisdictional claims in published maps and institutional affiliations.

Open Access This article is licensed under a Creative Commons Attribution-NonCommercial-NoDerivatives 4.0 International License, which permits any non-commercial use, sharing, distribution and reproduction in any medium or format, as long as you give appropriate credit to the original author(s) and the source, provide a link to the Creative Commons licence, and indicate if you modified the licensed material. You do not have permission under this licence to share adapted material derived from this article or parts of it. The images or other third party material in this article are included in the article’s Creative Commons licence, unless indicated otherwise in a credit line to the material. If material is not included in the article’s Creative Commons licence and your intended use is not permitted by statutory regulation or exceeds the permitted use, you will need to obtain permission directly from the copyright holder. To view a copy of this licence, visit <http://creativecommons.org/licenses/by-nc-nd/4.0/>.

© The Author(s) 2024